ATMOSPHERIC ENVIRONMENT: X 14 (2022) 100165

Contents lists available at ScienceDirect

Atmospheric Environment: X

journal homepage: www.journals.elsevier.com/atmospheric-environment-x

Source identification of the elemental fraction of particulate matter using size segregated, highly time-resolved data and an optimized source apportionment approach

M. Manousakas [a,*], M. Furger [a], K.R. Daellenbach [a], F. Canonaco [b], G. Chen [a], A. Tobler [a,b], P. Rai [a], L. Qi [a], A.H. Tremper [c], D. Green [c,d], C. Hueglin [e], J.G. Slowik [a], I. El Haddad [a], A.S. H. Prevot [a,**]

[a] Paul Scherrer Institute, Laboratory of Atmospheric Chemistry, 5232, Villigen, PSI, Switzerland
[b] Datalystica Ltd., Park InnovAARE, 5234, Villigen, Switzerland
[c] MRC Centre for Environment and Health, Environmental Research Group, Imperial College London, UK
[d] NIHR HPRU in Environmental Exposures and Health, Imperial College London, UK
[e] Laboratory for Air Pollution and Environmental Technology, Swiss Federal Laboratories for Materials Science and Technology (Empa), Überlandstrasse 129, 8600, Dübendorf, Switzerland

ARTICLE INFO

Keywords:
Source apportionment
PMF
Xact
Elemental composition

ABSTRACT

Source emissions with high covariance degrade the performance of multivariate models, and often highly-time resolved data is needed to accurately extract the contribution of different emissions. Here, we use highly time-resolved size segregated elemental composition data to apportion the sources of the elemental fraction of PM in Zürich (May 2019–May 2020). For data collection, we have used an ambient metals monitor, Xact 625i, equipped with a sampling inlet alternating between $PM_{2.5}$ and PM_{10}. By implementing interpolation and a newly proposed uncertainty estimation methodology, it was possible to obtain and use in PMF a combined dataset of $PM_{2.5}$ and PM_{coarse} ($PM_{10\text{-}2.5}$) having data from only one instrument. The combination of the inlet switching system, the instrument's high time resolution, and the use of advanced source apportionment approaches yielded improved source apportionment results in terms of the number of identified sources, as the model, additionally to the diurnal and seasonal variation of the dataset, also utilizes the variation from the size segregated data. Thirteen sources of elements were identified, i.e., sea salt (5.4%), biomass burning (7.2%), construction (4.3%), industrial (3.3%), light-duty vehicles (5.4%), Pb (0.7%), Zn (0.7%), dust (22.1%), transported dust (9.5%), sulfates (15.4%), heavy-duty vehicles (17%), railway (6.6%) and fireworks (2.4%). The Covid-19 lockdown effect in PM sources in the area was also quantified. High-intensity events disproportionally affect the PMF solution, and in many cases, they are getting discarded before analysis, removing thus valuable information from the dataset. In this study, a three-step source apportionment approach was used to get a well-resolved unmixed solution when firework data points were included in the analysis. This approach can also be used for other sources and/or events with very high contributions that distort source apportionment analysis. Optimized source apportionment techniques are necessary for effective air pollution monitoring.

1. Introduction

Aerosols, or airborne Particulate Matter (PM), have been the point of focus for many studies over the last decades. PM is a complex mixture of chemical species, originating from a variety of sources, both anthropogenic (traffic, industrial activities, and combustion processes in general) and natural (wind-blown dust, sea salt, forest fires, volcanic eruptions), and can be emitted as primary pollutants or formed as secondary products through atmospheric processes from gaseous precursors (Seinfeld and Pandis, 1998). Studies around PM are focused on many different subjects, such as their formation, chemical characterization, composition, and properties, as well as their impact on human health,

* Corresponding author.
** Corresponding author.
E-mail addresses: manousos.manousakas@psi.ch (M. Manousakas), andre.prevot@psi.ch (A.S.H. Prevot).

https://doi.org/10.1016/j.aeaoa.2022.100165
Received 1 December 2021; Received in revised form 18 March 2022; Accepted 19 March 2022
Available online 30 March 2022

climate, and visibility (e.g., Crippa et al., 2013; Daellenbach et al., 2020; Hallquist et al., 2009; Pandis et al., 1993; Pey et al., 2013; Rohr and Wyzga, 2012; Smith and Bond, 2014; Tobler et al., 2020).

Source apportionment (SA) is the practice of identifying and quantifying pollution sources. The SA of PM in an urban environment is a challenging task. Many anthropogenic and natural emissions need to be identified and quantified to effectively understand the corresponding atmospheric processes and mitigate the adverse effects of aerosols. Since most of those emissions usually occur inside the urban agglomeration and have similar chemical fingerprints in some cases (e.g., natural dust and construction dust, diesel and gasoline cars etc.), it is challenging for SA models to identify and distinguish them.

Additionally, since traditional SA methods are based on sample collection (usually 24h samples) (Manousakas et al., 2021; Viana et al., 2008), the time resolution of the results is low, and critical information regarding the diurnal cycles or particular short-lasting pollution events are either lost or hard to identify. In multivariate analysis, source emissions with high covariance may degrade the quality of the results since the models effectively use the variation between the source emissions for the source separation. The lower the sample's time resolution, the harder it is to include enough variation into the dataset since, in this case, the primary source of variation is mainly the seasonal variation. By contrast, when the time resolution is high (1h or less), the diurnal variation of the source emissions is also significant. Even short-lasting events and/or changes in the local meteorology can add to the overall variation of the dataset. Including in the dataset variables with different size ranges can also add extra variation and improve the results. Size-differentiated composition data permits more accurate estimation of emission processes and source fingerprinting.

Receptor models (RMs) are used to estimate the source contributions and fingerprints using multivariate analysis to solve a mass balance equation (Belis et al., 2015). The most commonly used receptor model is Positive Matrix Factorization (PMF) (Paatero and Tappert, 1994). PMF solutions describe the complex, time-dependent aerosol composition as a linear combination of factor profiles and their contributions. PMF has been successfully used in many studies around the world for the identification of the sources of the organic or/and inorganic fraction of PM (Amato and Hopke, 2012; Canonaco et al., 2015; Daellenbach et al., 2016; Kim et al., 2003; Manousakas et al., 2020). PMF results often have high uncertainty due to rotational ambiguity, wherein multiple solutions may have similar goodness of fit (Paatero et al., 2002). It is a common practice that the results from just a single run are reported in many PMF studies, even though it is found that in many cases, the uncertainty of a single solution can be very high, either due to rotational ambiguity and/or other reasons (Manousakas et al., 2017). An improved method for both uncertainty estimation and factor resolution was demonstrated by (Canonaco et al., 2013, 2021; Daellenbach et al., 2016, 2017), where rotational exploration and control were implemented by introducing *a priori* information about the source profiles to the receptor model. This methodology has been widely used since, but mainly in studies referring to the organic fraction of PM (e.g., Canonaco et al., 2015; Crippa et al., 2014; Qi et al., 2019; Stefenelli et al., 2019). Until recently, SA studies of highly time-resolved PM elemental composition data were limited (Angyal et al., 2021; Forello et al., 2019; Peré-Trepat et al., 2007; Pokorna et al., 2015; Pokorná et al., 2016; Richard et al., 2011; Visser et al., 2015). The samples for those studies were collected mainly by Streaker sampler (Annegarn et al., 1996; Lucarelli et al., 2011; Mazzei et al., 2007; Reizer et al., 2021), and by Rotating Drum Impactors (Raabe et al., 1988) and analyzed by accelerator-based analytical techniques (Prati et al., 1998).

Recent technological advances allowed for the development of instruments that have built-in analytical capabilities for online analysis of PM samples, with the potential to quantify ambient levels of elements with hourly or sub-hourly time resolution (Hasheminassab et al., 2020). One such commercially available instrument is Cooper Environmental's Xact 625i Ambient Metals Monitor. The Xact provides *in situ* automated measurements of ambient PM_{10}, $PM_{2.5,}$ or PM_1 elemental concentrations for a user-defined set of 24 or more elements with a user-selected sampling time resolution of 15–240 min (Furger et al., 2017; Tremper et al., 2018). SA of high-time resolution elemental data enables resolution of sources contributing to episodic and/or exceptional air pollution events. Several studies have utilized Xact data for PM source identification (Hasheminassab et al., 2020; Liu et al., 2019; Rai et al., 2019, 2020, 2021a; Wang et al., 2018, 2021; Yu et al., 2019), but most of them include data for relatively short time periods (maximum two months), and/or do not include size-segregated data. The Xact 625i is delivered with a "single size mode" inlet configuration (PM_{10}, $PM_{2.5,}$ or PM_1), where the latter is achieved by adding a $PM_{2.5}$ or PM_1 cyclone in series to the PM_{10} head. Consequently, in the original design, the Xact is operated in a single-size mode. Recently, Furger et al. (2020) developed an automated alternating inlet switching system for the Xact, allowing for the alternating collection of $PM_{2.5}$ and PM_{10} samples using a single instrument.

This study aimed to identify the sources of PM elements in Zürich, Switzerland, using size-segregated elemental composition data. PMF analysis was performed using a combined dataset of $PM_{2.5}$ and PM_{coarse} ($PM_{10\text{-}2.5}$). PM_{coarse} were estimated using the asynchronous $PM_{2.5}$ and PM_{10} data from a single Xact. The high-time resolution of the elemental data coupled with the size-segregated information led to improved SA results, which made the identification of 13 p.m. sources possible. Air pollution monitoring goes towards (near) real-time evaluation of source emissions. This is only possible if we first reach full characterization of the SA processes using high-time resolution elemental data in urban environments.

2. Instrumental and experimental

2.1. Sampling and instrumentation

Measurements were performed at an urban background site in Zürich (Zürich-Kaserne) (Fig. 1). Swiss environmental policy has achieved many successes since the 1980s and reduced the pollution of the environment by certain contaminants. As a result, the country's air quality has improved considerably over the past 25 years. According to the Research Institute of Organic Agriculture (FiBL), Zurich, as well as the larger metropolitan or peri-urban area, which covers most of the Canton Zurich area and parts of Canton Aargau (with Baden as larger town), is an economically booming region in Switzerland. Most of the main large companies are located in or near Zurich. As a result, there is a strong pressure on agricultural land. The communities and smaller towns near the city (10–20 km around) are very much oriented towards Zurich with many of their inhabitants working in the city increasing car traffic in the city.

The instruments deployed for this campaign were a Q-ACSM (Ng et al., 2011), an AE33 aethalometer (Drinovec et al., 2015), a total carbon analyzer (TCA08) (Rigler et al., 2020), and an Xact 625i ambient metals monitor (Furger et al., 2017). The station started operation on May 7th, 2019, and was dismantled on May 29th, 2020 (including the Covid-19 lockdown period). In late February, the Covid-19 pandemic reached Switzerland. As the situation aggravated in March, the Federal Council declared a country-wide lockdown and other stringent measures starting on March 16, 2020, bringing much of the economic activities to a halt. With people staying at home, commuting traffic was reduced substantially, and empty roads were the picture of the day. Air traffic was reduced by more than 90%. Many employees worked in home-office, and goods were ordered online and delivered by mail only, as many shops were closed. The gradual easing of the measures slowly increased traffic and industrial activities. The lockdown was ended on May 11, 2020, though many businesses and events were still prohibited.

The site, a courtyard, is considered an urban background location and also contains a permanent monitoring station for the NABEL network. The data retrieved from NABEL were used either for validation

Fig. 1. The sampling point and central train station (right) in Zürich, Switzerland (left).

or/and as auxiliary information. The parameters that were used in the study were SO_2 (Thermo 43i), NO_x (Horiba APNA 370), O_3 (Thermo 49i), CO (Horiba APMA 370), $PM_{2.5,}$ and PM_{10} (PALA Fidas 200). Some restaurants exist in the immediate vicinity, but the station is shielded from the surrounding roads by long buildings on all sides. Zürich central train station is located about 300 m to the northeast. The site has been characterized previously in multiple publications (Canonaco et al., 2013, 2015; Daellenbach et al., 2017; Hueglin et al., 2005; Lanz et al., 2008; Qi et al., 2019; Stefenelli et al., 2019).

$PM_{2.5}$ and PM_{10} concentrations of 37 elements (Al, Si, P, S, Cl, K, Ca, Sc, Ti, V, Cr, Mn, Fe, Co, Ni, Cu, Zn, Ga, Ge, As, Se, Br, Rb, Sr, Y, Zr, Nb, Cd, In, Sn, Sb, I, Ba, Hg, Tl, Pb, Bi) were measured in 1-h intervals with an Xact 625i ambient metals monitor from May 17th, 2019 until May 20th, 2020. Briefly, the air is sucked through a filter tape with a flow rate of 16.7 lpm for a 1-h sampling interval; then, the tape is moved to the analysis area, where it is excited using an x-ray source (Rhodium anode, 50 kV, 50Watt) in three successive energy conditions, which target three different suites of elements. The resulting x-ray fluorescence is measured with a silicon drift detector, and the spectra are analyzed using a proprietary spectral analysis package that takes into account all peaks associated with a given element. During the analysis time, the next sample is collected; finally, the cycle is repeated. The accuracy of the measurements has been determined for the forerunner instrument, Xact 625 (Furger et al., 2017; Tremper et al., 2018). As mentioned earlier, the instrument used in Zürich was equipped with an inlet switching system (Furger et al., 2020), which allowed for alternating sampling of PM_{10} and $PM_{2.5}$. For quality control, Xact measurements were compared with ICP-MS/OES. The average deviation of Xact values from filter measurements analyzed with ICP-MS/OES was 30% (Furger et al., 2017). Detection limits of the Xact 625i and quality control data are presented in the supporting material.

Organic aerosols were measured with an Aerodyne Aerosol Chemical Speciation Monitor (ACSM) with 10 min resolution. The system used was a Q-ACSM system (Ng et al., 2011), equipped with a $PM_{2.5}$ inlet. For the measurements of Total Carbon (TC) and Organic Carbon (OC), the TCA08 Total Carbon Analyzer from MAGEE Scientific was used (Massabò and Prati, 2021; Rigler et al., 2020), providing information every 1-h. TCA08 uses a thermal method for TC determination. It collects a sample of atmospheric aerosols on a 47-mm diameter quartz fiber filter enclosed in a small stainless-steel chamber at a controlled sampling flow rate. It has two parallel sampling and analysis channels. While one channel is collecting its sample for the next time-based period, the other channel is analyzing the sample collected during the previous period. Finally, for eBC (equivalent Black Carbon) measurements, the Aethalometer model AE33 was used (Drinovec et al., 2015), in 1-min resolution.

The contributions to eBC from fossil fuel combustion (eBC_{ff}) and biomass burning (eBC_{bb}), the measured absorption coefficients at wavelengths 470 and 880 nm were estimated using the alpha values reported in Zotter et al. (2017), ($a_{tr} = 0.9$ and $a_{wb} = 1.68$).

The NABEL station provided meteorological, air quality data that were used for intercomparisons and quality testing and complementary to the measurements conducted in the frameworks of the study.

2.2. Setting up PMF analysis

Information about the theoretical base of PMF are provided in the "PMF analysis" section in the SI. A common approach for the choice of species to include in the PMF input depends on the percentage of data below the detection limit (Polissar et al., 1998). Elements with more than 70% (assessed separately in each size fraction) of their measured time points below the interference-free one sigma MDL (minimum detection limit) were excluded from further analysis if they were not considered important tracers of specific sources. In the end, 25 elements (out of the 37) were used (Al, Si, S, Cl, K, Ca, Ti, V, Cr, Mn, Fe, Ni, Cu, Zn, As, Se, Br, Rb, Sr, Zr, Sn, Sb, Ba, Pb, Bi) from the $PM_{2.5}$ fraction and the same elements for the coarse fraction, resulting in 50 variables in total. Similar to (Rai et al., 2020), all the entries in x_{ij} with a signal-to-noise ratio (SNR) below 2 were down-weighted by replacing the corresponding s_{ij} with a penalty function $2/SNR_{ij}$ (Visser et al., 2015).

As described before, the Xact system used during the campaign was equipped with an inlet switching system, which offers the advantage of providing alternating $PM_{2.5}$ and PM_{10} elemental concentration measurements (denoted here as $PM_{el\text{-}2.5}$ and $PM_{el\text{-}10}$). Several approaches were attempted for the accurate estimation of PM sources based on the elemental content of PM. At first, the $PM_{el\text{-}10}$ and $PM_{el\text{-}2.5}$ datasets were used separately as well as combined together to perform the PMF runs. By using the aforementioned approaches, six to nine sources could be identified, with the number being the highest (nine identified sources) when $PM_{el\text{-}10}$ data were included in the dataset. This indicates that sources that produce coarse particles are relevant in the area, and including this information improves the solution. The separate runs had

the disadvantage of including the information of either $PM_{el\text{-}10}$ or $PM_{el\text{-}2.5}$, and in both cases, information about $PM_{el\text{-}coarse}$ is either not present ($PM_{el\text{-}2.5}$), or represents a percentage of the total mass ($PM_{el\text{-}10}$). From the initial runs, it was concluded that the SA process would improve if $PM_{el\text{-}coarse}$ were used in the dataset.

In this study, a new approach for calculating continuous PM_{coarse} fraction ($PM_{10\text{-}2.5}$) was used. The first step was to produce continuous measurements for each fraction by linear interpolation of the existing data points. Interpolation was perfomed only for missing points owed to the alternating sampling system, and not data gaps. $PM_{el\text{-}coarse}$ was then calculated by subtracting the continuous $PM_{el\text{-}2.5}$ from $PM_{el\text{-}10}$ and was used with $PM_{el\text{-}2.5}$ as PMF input. For some rare cases that $PM_{el\text{-}coarse}$ were estimated as negative values ($PM_{el\text{-}2.5} > PM_{el\text{-}10}$), the reported value was substituted by zero, and a very high uncertainty was assigned to the point. In all cases that negative values were observed, the $PM_{el\text{-}2.5}/PM_{el\text{-}10}$ was almost equal to 1, meaning that practically the concentrations were almost equal, and the (slightly) negative values were observed due to the measuring uncertainty of the instrument and the interpolation uncertainty. For that reason, it was concluded that assuming a $PM_{el\text{-}coarse}$ equal to zero for those points is a valid assumption.

The uncertainty of the measurements was calculated according to the methodology described by (Reff et al., 2007):

$$S_{ij} = \sqrt{(p_j \times x_{ij})^2 + (MDL_j)^2} \quad (4)$$

where x_{ij} indicates the elements of the data matrix, while subscripts i and j are indices for time and elements. In this study, an estimated analytical uncertainty (p_j) of 10% was used to derive the error matrix dataset (Rai et al., 2019). Values that were much lower than the DL (only the negative and zero values) were substituted by ½ DL, and the uncertainty was set as 5/6 of the DL value (Reff et al., 2007). As it is suggested by Brown et al. (2015), the substitution of all BDL values by replacement values, such as ½ DL, when the original measured values are available, has no proven advantages because the species with low SNR are down-weighted in the modeling process.

Another important point is the uncertainty propagation of the interpolated points. Linear interpolation involves an averaging of adjacent points, thus, within a specified measurement interval, the concentration of the interpolated point is bounded by the first and last markers/hours of the interval for a given size mode (x) of PM;

$$PM_{x,mid} = ½ * (PM_{x,first} + PM_{x,last}) \quad (5)$$

The uncertainty of this mid-point interpolation is estimated by variance pooling:

$$Unc\_PM_{x,mid} = \sqrt{Unc^2_{x,\,first} + Unc^2_{x,\,last}} \quad (6)$$

While the interpolation approach made it possible to construct a continuous dataset with information for both fine and coarse elemental concentrations, it also introduces uncertainty in the analysis. This uncertainty is linked to how well the 12h average concentration of each element compares to the 24h average that would have been estimated if the sampling changing inlet was not used. Even though the data were used in their native 1h time resolution, since it is impossible to know the concentration of the non-measured point, the 24h average was used as a metric of the comparison between the measurements with and without the sampling changing inlet. Furger et al. (2020), investigated the uncertainty of the sample changing inlet to the average concentration of each element by using continuous data to simulate the alternating sampling cycle. The simulated results were compared to the actual continuous data for each element. The investigation showed average differences of <5% for all measured elements, except for Mo, Cr, and Ni, where differences reached 8.8%, 22%, and 38%, respectively (Furger et al., 2020). Additionally, it was concluded that the uncertainty depends on the $PM_{2.5}/PM_{10}$ ratio of each element (the lower the ratio, the higher the uncertainty). Even though the uncertainty estimated in Furger et al. (2020), refers to the average elemental concentration, it is equivalent to that of the interpolated points, since in both cases, it is attributed to the missing points in the dataset.

Since every point of the PMF dataset is weighted by the corresponding uncertainty, and down-weighted points are less important to the analysis, points with higher uncertainty can be included without perturbing the results if a realistic uncertainty is assigned to them. Due to the interpolation approach used, if the increase/decrease in the concentration of the interpolated point is non-linear, the point will not be estimated accurately. Additionally, regardless of the interpolation approach used, if a high-intensity 1h event takes place, it is impossible to be modeled right in a systematic way. This observation is consistent with Furger et al. (2020), which concluded that "spikes" in the time series increase the uncertainty. Since linear interpolation was the selected method, the variability of the ambient concentrations is not possible to be predicted if a sharp increase/decrease in the concentrations takes place. Sharp increases (plumes or/and local pollution events etc.), even though not very common, can disproportionately affect the results of PMF.

Three approaches were explored to estimate a scaling factor of the uncertainty of the interpolated points accurately. The first approach was to include the uncertainty estimated by (Furger et al., 2020) in equation (4) on an element-by-element basis. The disadvantage of this approach is that all points are equally down-weighted, while in reality, the uncertainty is almost exclusively increased by a few points that correspond to events that are not adequately estimated by the interpolation procedure. Further, the uncertainties calculated by Furger et al. are specific to that measurement site (kerbside site in London) and time period and may differ greatly from the current study. The second approach was based on the estimation of the standard deviation of two consecutive real points compared to the average for the entire time series. The idea behind that approach was that if the deviation was high for a specific set of points, that corresponds to a sharp increase/decrease between two real measurements, and thus a higher probability of inaccurate estimation of the intermediate interpolated point. This approach yields satisfactory results only if the increase between two points is sharp and non-linear, but it falls short if the increase is sharp but linear (false high uncertainty), or lasts less than 1h (false low uncertainty).

The third (and used) approach for estimating a scaling factor for the uncertainty of the interpolated points was based on the $PM_{el\text{-}2.5}/PM_{el\text{-}10}$ ratio. Briefly, the uncertainty was calculated as: the $PM_{el\text{-}2.5}/PM_{el\text{-}10}$ ratio of every time step (for each element) in the dataset was estimated using the $PM_{el\text{-}2.5}$ concentration value of that point and the average $PM_{el\text{-}10}$ concentration value of the previous and the next point (or the opposite if the time point corresponding to a $PM_{el\text{-}10}$ measurement). Then the ratio was compared with the average ratio of the whole time series of that particular element ($avg(PM_{2.5}/PM_{10})$); if it was not within two standard deviations, then the uncertainty of that point was down-weighted by a factor of three. Generally, in PMF, even a small amount of overweighting is quite harmful and should be avoided, while in contrast, moderate down-weighting, by a factor of two or three, does not create strong modeling errors and sometimes is useful if the user is not sure if high values in the dataset correspond to an actual event (Paatero and Hopke, 2003). This approach is the only approach that can estimate if a sharp increase or decrease occurs in the time series. As stated before, the "gaps" in one size fraction dataset corresponds to measured points in the other fraction. By using the $PM_{el\text{-}2.5}/PM_{el\text{-}10}$ the estimation of the interpolated points' uncertainty is based on actual data from the other size fraction.

In PMF analysis, the step that involves the highest uncertainty is selecting the number of factors. The optimum approach involves mathematical diagnostics (Q/Q_{exp}, scaled residuals, structure of the residuals, unexplained variation), as well as the examination of the physical meaning of the factors based on several indicators e.g., diurnal variations, correlation to external data, time series analysis.

The first step was examining unconstrained solutions from five to

fifteen factors, including the data from the entire time period. However, preliminary analysis of these solutions indicated persistent mixing across factors. This mixing appeared due to the presence of a fireworks factor. Fireworks presented a non-negligible contribution throughout the year. Additionally, Sulfates, Salt, and Biomass factors had apparent mixing during the firework event days, showing unreasonably large spikes in their contributions. Those spikes that coincide with the firework events, and especially for transported sources that are not expected to have stable contributions in a short time, do not have any physical explanation and are the product of the mixed PMF solution. A similar difficulty was observed in the study of Rai et al., (2019), where the authors explained that due to the very high SNR, during the fireworks events (owed to the extremely high concentrations), any model imperfection has a strong influence on Q, and the model compensates for that by assigning mass to other factors. Therefore, the PMF analysis was conducted in several steps.

To avoid having a mixed solution, a new set of input matrices were constructed containing only points with negligible contributions from fireworks (non-firework points, NFP). The fireworks points in the dataset were defined by knowledge of the area (known days that fireworks were used), and were confirmed by examining the time series of Bi, K, and S concentrations (values higher than two standard deviations from the average). PMF analysis of the NFP dataset was conducted on solutions containing five to fifteen factors, without any constraints applied. For each selected number of factors, 50 randomly initialized runs ("seeds") were conducted. The criteria for the optimum number of factors selection were the interpretability of the factors and the mathematical indicators. A commonly used approach to select the number of factors is to assess the Q/Q_{exp} as a function of the number of factors to evaluate the extent to which each additional factor improves the explanation of the overall dataset variation. The Q/Q_{exp} gradually decreased from ~2.5 to ~1 for eleven factors (Fig. S.14.), and the decrease rate was reduced from that point, indicating that the optimum solution was around that number. We selected a twelve factor solution as the best representation of the data (i.e., the highest number of factors for which each factor could be physically interpreted). The benefit from using twelve factors instead of eleven was that railway emissions, rife in this area, were identified (Bukowiecki et al., 2007; Ducret-Stich et al., 2013; Gehrig et al., 2007). The scaled residual (over the time series and variables) in this solution was within the range of ±3, with very small values (Fig. S6.). The real unexplained variation decreased from 10% for a 5-factor solution to 5% for the 12-factors solution.

Then, the profiles of factors retrieved from the analysis of the NFP dataset were tightly constrained (a = 0.05) within a second PMF analysis of the full dataset, including firework points (FP). However, this analysis yielded unmixed source profiles but time series that were mixed similarly to the entire dataset solution (Fig. S7.). Therefore, a second FP analysis was conducted in which both the source profiles and the time series were tightly constrained based on the NFP results. To utilize the time series retrieved from NFP PMF for PMF of the FP dataset, it is necessary to estimate concentrations for the NFP-derived factors during fireworks events (FE). This was done as follows. First, the background concentrations of all other sources were calculated for the firework data points. The calculation was based on the average diurnal variations of the source contributions. At first, the average source contribution at 12:00 (local time) was selected as a reference point (due to low standard deviation during that time), and the ratio of the average concentration of every hour to that of 12:00 was estimated based on the average diurnal variation of each source. Then, the source contributions during FE of all sources were estimated based on the contribution of each source at 12:00 during the FE days. Using that approach, we estimated the 113 points that correspond to the FE, in the 7608 total points included in the dataset. We then ran the model tightly constraining the source profiles of the original 12 sources (a = 0.05), and the time series of all 13 sources (a = 0.05). Fireworks time-series were constrained to zero except during FE, where they were left random/free. The fireworks source profile was left entirely unconstrained. If more than 13 sources were used, the fireworks factor was unreasonably split. In this case as well, the scaled residual (over the time series and variables) of the solution was within the range of ±3, with small values (Fig. S8.).

It should be noted here that before selecting an a-value of 0.05 to constrain the solution, we performed a sensitivity analysis using a-values ranging from 0.05 to 0.4. Because of the extremely high concentration of the firework tracers during the FE, all sources with similar tracers showed a spike at the same time as fireworks, which is clearly resulting from mixing. Only very low a-values allowed for unmixed solutions. To validate the performance of the used methodology, we set two criteria: a) the average contribution of all other sources but fireworks should not change significantly when the firework points are introduced in the dataset (since they are a minor fraction of the dataset), and b) the firework factors profile retrieved should be in accordance to the ones reported in the bibliography. Criterion a was evaluated by comparing the average source contribution of FP and NFP solutions, which were found to be almost identical. Criterion b is especially important since, by tightly constraining the solution to meet the original NFP solution, what is done practically is that the extra mass due to the FE points is apportioned to an extra factor. If this factor is well resolved and not mixed, then the assumption that all the extra mass was originating from it is validated. In the end, the used approach led to a well-resolved solution with low scaled residuals for all variables and time points (Fig. S.8.), unmixed time-series (Fig. S.12.), and a very well-defined firework's source profile, in excellent agreement with the previously reported elemental ratios, K/S elemental concentration ratio (~2.76) in black powder and the Ba/K ratio (more details in the results section) (Dutcher et al., 1999; Pongpiachan et al., 2018; Rai et al., 2019).

The uncertainty of the NFP solution was estimated using a method based on a combination of the a-value approach (information about the rotational ambiguity) and the classical bootstrapping approach (information about the statistical uncertainty and random errors), as proposed by (Canonaco et al., 2013). The results and the approach are described in detail in the supporting material.

2.3. Concentration Weighted Trajectories, CWTs

To identify the spatial origin of the aerosol components, air mass back-trajectories arriving at the station have been analyzed by statistical methods. For the analysis of the back trajectories, the Openair package was used (Carslaw and Ropkins, 2012). Openair is an R package primarily developed for the analysis of air pollution measurement data but which is also of more general use in the atmospheric sciences. The trajectories were calculated using the NOAA (National Oceanic and Atmospheric Administration) HYSPLIT 4.0 model (Rolph et al., 2017; Stein et al., 2015). The model calculation method is a hybrid between the Lagrangian approach, using a moving frame of reference for the advection and diffusion calculations as the trajectories or air parcels move from their initial location, and the Eulerian methodology, which uses a fixed three-dimensional grid as a frame of reference to compute air pollutant concentrations (Stein et al., 2015).

120-h backward air mass trajectories (BWT) arriving at the location of the sampling site were computed using global data assimilation system (GDAS) meteorological files. The data have a spatial resolution of 1-degree longitude and latitude. Detailed information regarding the GDAS database is provided in Stein et al. (2015) and the NOAA Atmospheric Research Laboratory website. The BWT were computed every 3 h (ending at 00:00, 03:00, 06:00, 09:00, 12:00, 15:00, 18:00 and 00:00 UTC hours) for each day of the period of study at 500 m above ground level (agl).

To clarify the spatial distribution of sources that affected the concentrations of chemical components at the sampling sites, the method of Concentration Weighted Trajectories (CWTs) (Seibert et al., 1994) was used. Each grid cell gets a weighted concentration obtained by averaging

sample concentrations that have associated trajectories that crossed that grid cell as follows:

$$\ln(\overline{C}_{ij}) = \frac{1}{\sum_{k=1}^{N} \tau_{ijk}} \times \sum_{k=1}^{N} \ln(C_k)\tau_{ijk} \quad (7)$$

where i and j are the indices of the grid, k the index of trajectory, N the total number of trajectories used in the analysis, C_k the pollutant concentration measured upon arrival of trajectory k, and τ_{ijk} the residence time of trajectory k in grid cell (i, j). A high value of C_{ij} means that air parcels passing over the cell (i, j) would, on average, cause high concentrations at the receptor site.

3. Results

3.1. Daily PM composition and meteorological conditions

The field campaign covered eight months in 2019 and 5 months in 2020. 2019 was the 5th warmest year on record, with the 3rd warmest summer and the 6th warmest autumn (MeteoSchweiz, 2020a). Starting with a cooler-than-normal May, June and July experienced two heatwaves with temperatures above 30 °C and sunshine durations above normal. Interestingly enough, precipitation was not much below average (80–100%). Winter 2019–2020 was the warmest on record, with an average temperature above 0 °C for Switzerland (MeteoSchweiz, 2020b). During spring of 2020, Zurich obtained 50–60% of the average precipitation (MeteoSchweiz, 2020b).

Basic weather parameters measured with the Xact sensors are shown in Fig. 2.

The heatwaves affected the measurements during the field campaign. As the instruments were mounted in an old trailer, the air conditioning unit was sometimes overstrained, leading to a temperature-related shut-down of the Xact.

The mean values and standard deviations of the hourly data for the whole campaign were for SO_2 0.67 ± 0.47 μg m^{-3}, for NO_x 18.4 ± 18.4 ppb, for NO_2 18.9 ± 12.5 μg m^{-3}, for O_3 68.8 ± 25.0 μg m^{-3}, for CO 0.21 ± 0.05 mg m^{-3}, for PM_{10} 10.3 ± 6.9 μg m^{-3} and for $PM_{2.5}$ 7.3 ± 4.3 μg m^{-3}. NO_2 monthly mean values were below the EU annual limit value of 30 μg m^{-3} except for January 2020. This is probably related to the heating season, despite the apparent dip during the Christmas holidays, which may be due to reduced traffic on Christmas days. Of these parameters, only $PM_{2.5}$ exceeded the 24-hr limit. This occurred twice, in January 2020 and in April 2020. For many of the gas-phase parameters, there is a remarkable drop in concentrations from Jan to Feb 2020, which correlates well with the wet weather and higher wind speeds of February. A drop in the concentration of NO during the lockdown is not visible in March (20.9 μg m^{-3}), but lower average concentrations are recorded during April (17.3 μg m^{-3}) and May (13.2 μg m^{-3}) 2020. Additionally, O_3 presents higher than average concentrations during April (78.6 μg m^{-3}) and May (72.3 μg m^{-3}) 2020. The effect of the lockdown on $PM_{2.5}$ and PM_{10} concentrations is not apparent, as both fractions have lower than average concentrations during February 2020 (3.6 and 8.1 μg m^{-3}), and higher than average during March (7.5 and 12.9 μg m^{-3}) and April (9.7 and 15.1 μg m^{-3}).

The Xact 625i provided *quasi*-continuous elemental concentrations in ng m^{-3}, with only a few gaps due to instrument problems or inappropriate operating conditions (heatwaves). A statistical overview is given in Fig. 3. All calibrated elements are listed, even if the signals were noisy and mainly below the minimum detection limit (MDL). Si, S, Cl, K, Ca, Ti, Cr, Mn, Fe, Ni, Cu, Zn, As, Br, Sr, Ba, and Pb were on average above MDL for both sizes, Zr only for PM_{10}. Al, V, Co, Ga, Ge, Se, Rb, Y, Cd, In, Sn, Sb, I, and Bi were typically below MDL. For P, Sc, Hg, and Tl,

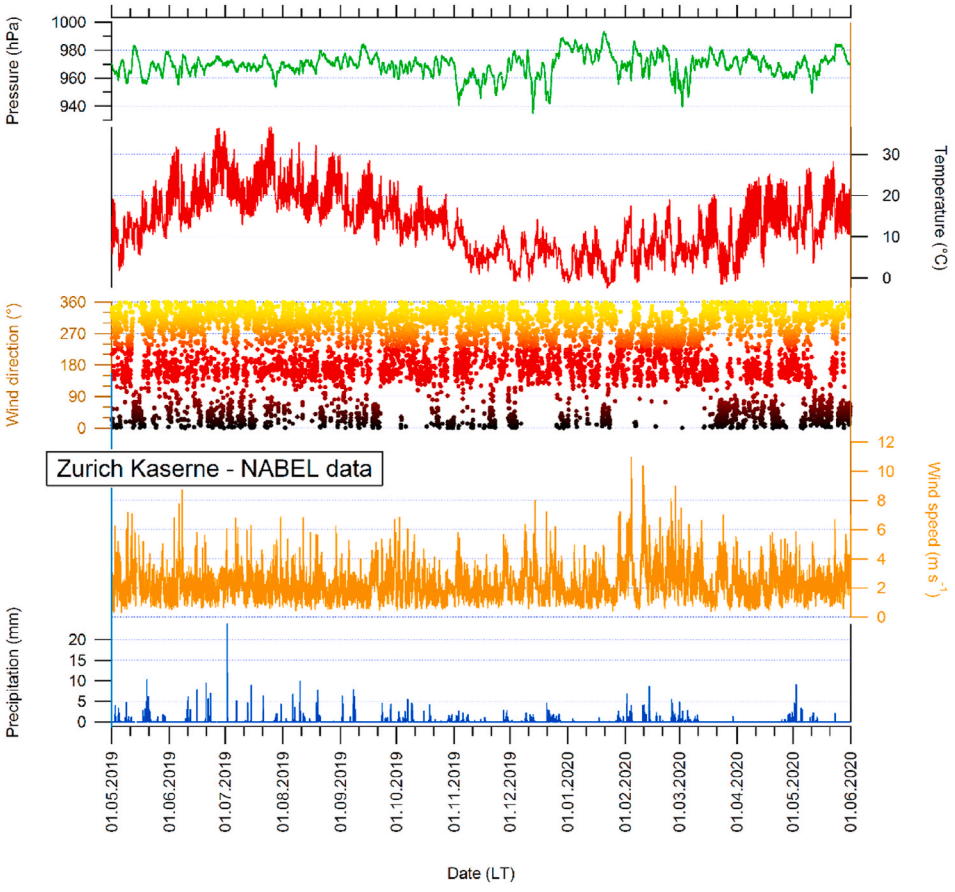

Fig. 2. Time series of pressure, temperature, wind direction, wind speed, and precipitation at the site Zurich Kaserne.

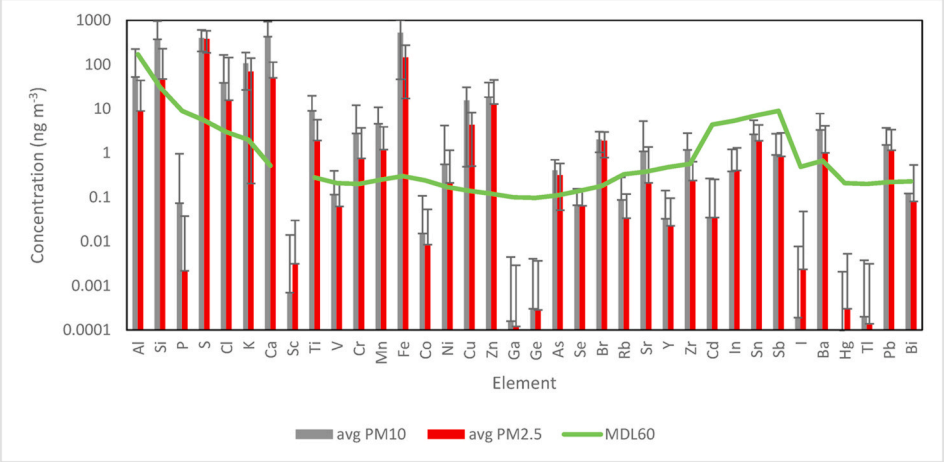

Fig. 3. Average concentrations of elements in PM_{10} and $PM_{2.5}$ for the whole campaign. The green line indicates the minimum detection limits (MDL) for 60-min sampling intervals (Table S.2.) and the error bars represent the standard deviation. (For interpretation of the references to color in this figure legend, the reader is referred to the Web version of this article.)

no MDL has been reported, but the observed average concentrations are likely also below MDL. Nevertheless, the below-MDL elements provided valuable, though spiky data that episodically exceeded the MDL. Such data can still be used for source apportionment when treated appropriately (Rai et al., 2020). Firework events such as the 2019 Zurich Pride Festival, the Zürich Fest, the Swiss National Day, and New Year's Eve yielded extremely high peak concentrations for some elements (S, K, Sr, Bi). The K $PM_{2.5}$ peak concentration on July 6, 2019 (Zürich Fest) reached 49 μg m^{-3}. Practically all elements show $PM_{el\text{-}10}$ to be larger than $PM_{el\text{-}2.5}$, as expected. The few exceptions (Sc, Ni, Ge, I, Hg, Ti) are either far below MDL on average or show a noisy behavior, hence this observation may be a measurement artifact (alternating sampling, Furger et al., 2020). The elements Fe, S, Ca, Si, K, Cl, and Al make up 96.6% of the mass of measured elements in $PM_{el\text{-}10}$, and 95.5% in $PM_{el\text{-}2.5}$. The average concentration of $PM_{el\text{-}10}$ is 2.38 μg m^{-3}, and of $PM_{el\text{-}2.5}$ is 1.01 μg m^{-3}, which accounts for 8.6% and 12.1% of PM_{10} and $PM_{2.5}$, respectively.

The element with the highest contribution to $PM_{el\text{-}10}$ is Fe and to $PM_{el\text{-}2.5}$ is S, with average concentrations of 545 ng m^{-3} and 406 ng m^{-3} respectively. In a previous study that took place at the same site in Zürich in 2008 (Richard et al., 2011), the authors reported higher concentrations for S, Cl, and K. This observation is consistent with the findings of Gianini et al. (2012b), that reported a decreasing trend in sulfate concentrations in Zürich, and in PM-related pollution of the area in general.

The European Commission, in a directive relating to toxic metals, has set assessment thresholds for Pb (1999/30/EC, 1999), As, Cd, and Ni (2004/107/EC, 2004). The mean annual concentration proposed for As is 6 ng m^{-3}, Ni is 20 ng m^{-3}, and Cd is 5 ng m^{-3}, all measured in PM_{10} fraction (2004/107/EC, 2004). For all elements, the concentrations in Zürich are well below the limit values.

The elements which are abundant mainly in the fine fraction are S and K, with both mean and median values substantially higher than in the coarse one. On the other hand, the mineral dust-related elements Al, Si, Ca, and Fe are higher in the coarse fraction of PM as expected. The diurnal variations, summary statistics, and the correlations of the element time series with external data are presented in the supporting material. The diurnal variations of some of the elements (Fe, Cu, As, Zr) have distinct double peaks in the morning and late afternoon, corresponding to traffic rush hours (Figs S4 and S5.) indicating a strong effect of vehicular movement on their concentrations in the area (Forello et al., 2019). Other elements often linked to the same source, Zn, Mn, and Pb, do not show a similar pattern. Regarding the correlations with the external data, K correlates well ($R > 0.6$) with CO, BC_{wb}, TC, and OC. NO_x has a high correlation (>0.6), with fine K, As, Rb, and coarse Fe, Cu, and Zr, which are a strong indication of traffic origin (Daellenbach et al., 2017). Finally, S and Cl correlate (>0.8) with NH_4^+ and SO_4^{2-} and Cl^- from the ACSM.

Six cases of very high PM concentrations (>60 μg m^{-3}) were recorded during the study period: a) July 5th, 2019, b) October 24th, 2019, c) November 16th, 2019, d) December 17th, 2019, e) January 1st, 2020, f) March 28th, 2020. Cases a and e are linked with fireworks shows during Zürich Fest (July 5th to 7th) and new year celebrations. PM_{10} concentrations were very high, 105.5 and 70.1 μg m^{-3} for the two events, with the $PM_{2.5}/PM_{10}$ ratio being almost 1. The PM components with high concentrations were fine K, S, Cl, Ba, Sr and Bi. In cases b, d, and f, PM_{10} concentrations were 62.3, 126.2, and 70.4 μg m^{-3}, with low $PM_{2.5}/PM_{10}$ (~0.3). The components with high concentration during those events were coarse Al, Si, Ca, and Fe, indicating a high contribution of mineral dust. Finally, during case c, the PM_{10} concentration was 73.6 μg m^{-3}, and the $PM_{2.5}/PM_{10}$ equal to 0.8. High concentrations of elemental Cl (14.7 μg m^{-3}) and non-refractory Cl (6.0 μg m^{-3}) and NH_4^+ (4.1 μg m^{-3}), were recorded during the time of the event. Due to the very high concentration of the refractory Cl, the event is probably linked with long-range transport of sea salt or road salt resuspension and is discussed in detail later.

3.2. Source apportionment results

3.2.1. Sea salt

The salt factor contributes significantly to fine Cl_f (70%), coarse Cl_c (98%), and coarse Br_c (32%) (Fig. 4.). The source corresponds to transported sea salt, and the variation in concentration is mainly driven by high-intensity events, a typical feature for advected sources. Generally, Cl concentrations are primarily affected by road salting or/and sea salt transportation (Mcnamara et al., 2020). Chlorine can also be emitted from other sources such as coal combustion, waste incineration, industrial emissions, and biomass burning (Jayarathne et al., 2017; Osto et al., 2013; Rai et al., 2021b), but none of those sources are relevant in this area. Coarse Cl_c does not correlate with any other element (with traffic origin or not), an indication that it originates from a distinct source, while fine Cl correlates with K, Ti, Cu, Sr, Ba, and Sb, owing to their common emissions from fireworks. When the entries that correspond to fireworks events are not included in the correlation analysis, fine Cl presents only a moderate correlation to Br_c. Based on those observations, it is assumed that the source corresponds to sea salt transportation, and road salting either does not affect or slightly affects the factor. In a prior study at several sites around Switzerland, de-icing

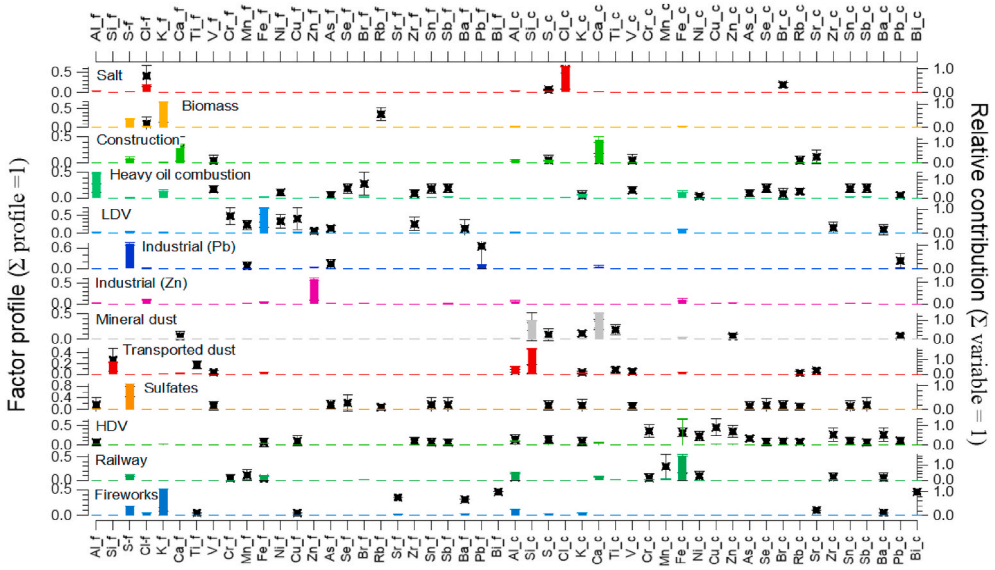

Fig. 4. Source profiles of the identified sources. The bars represent the normalized contribution of the tracers to the factor (left axis), and the star the normalized contribution of the factor to the tracer (right axis). The extension _c on the element names indicates the coarse fraction, and _f the fine fraction. The error bars correspond to the standard deviation of the solutions.

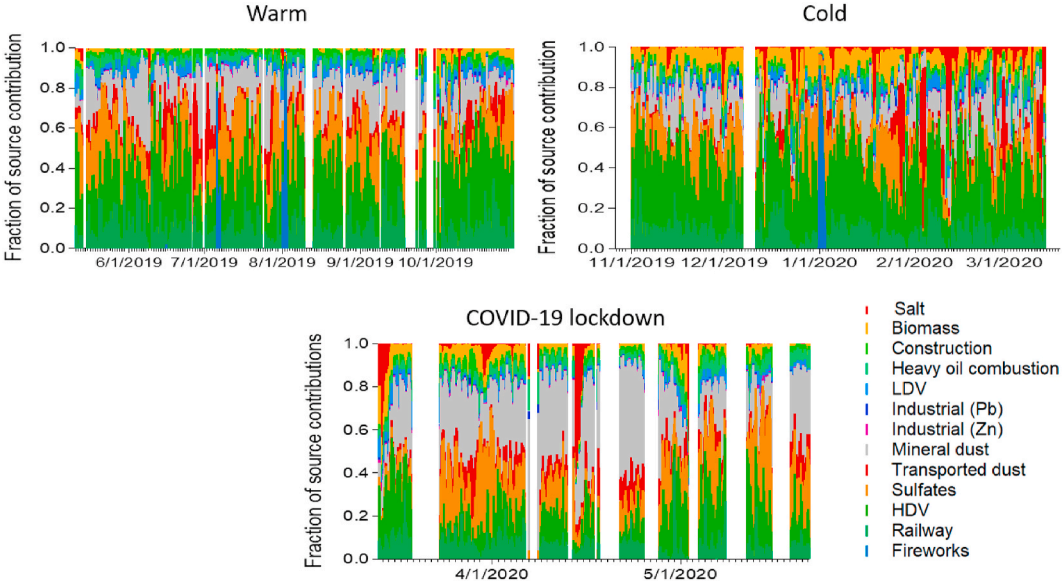

Fig. 5. Time series of the source contributions fractions.

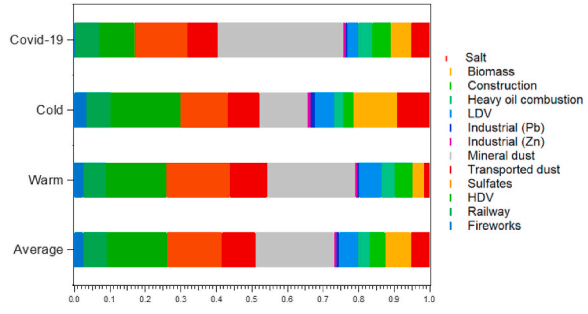

Fig. 6. Source contributions (per period) as a fraction.

road salt was identified only at a traffic site at Bern and not in Zürich (Gianini et al., 2012a). The comparison of the refractory and non-refractory (Xact and ACSM) Cl, presents high differences during high Cl concentration events. ACSM derived non-refractory Cl^{-}, is nearly insensitive to Cl from sea/road salt Cl. The effect of sea salt aerosols in Central Europe has been recorded in the past (Chen et al., 2016). The origin of the source was investigated further using trajectories statistical methods, and the results are presented in the following section. The diurnal variation of the source shows no clear pattern, as expected from a transported source, with a peak at 10:00 (Fig. 7), attributed to the very high Cl event recorded on November 16th, 2019 (Fig. 5.), at the same time. The average source contribution to PM_{el} is 5.4% (Fig. 6.) (1.7% during Warm and 9.3% during Cold season), and 75% is attributed to the coarse elements in the factors.

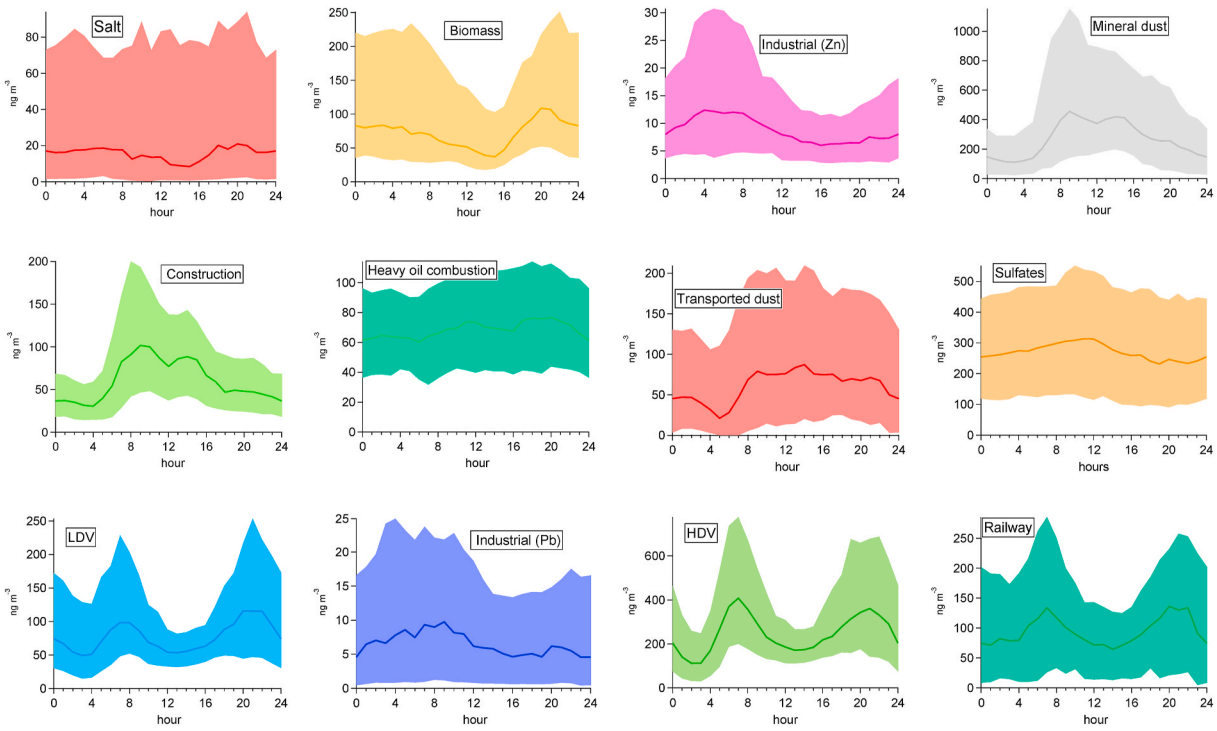

Fig. 7. Median diurnal variation of the source contributions in ng m^{-3}. The shaded area corresponds to the IQR (interquartile range).

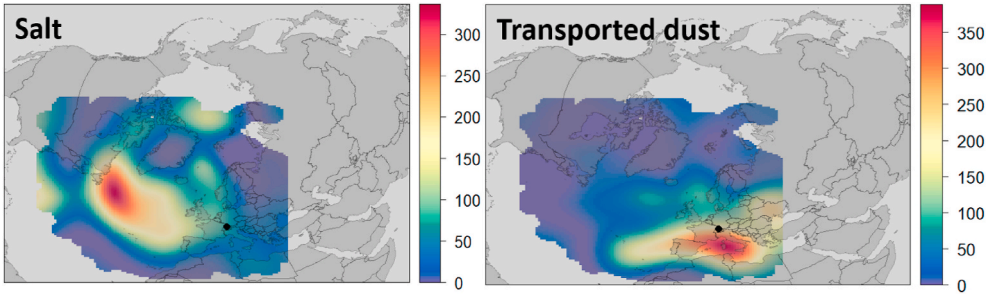

Fig. 8. CWTs for the two sources that are affected by long-range transport. The scale is in ng m^{-3}, and the color scale is relative to the highest contribution of each source. (For interpretation of the references to color in this figure legend, the reader is referred to the Web version of this article.)

3.2.2. *Biomass burning*

This factor contributes to K_f (67%), Rb_f (56%), Cl_f (16%), and S_f (10%). K is a well-known tracer of biomass burning (Amato et al., 2016; Heo et al., 2009), and water-soluble K, which is an inorganic compound mainly present in ash, is considered as the second-best tracer of this source after levoglucosan. Biomass burning is very relevant in Switzerland and is found to have a lower and rather homogeneous contribution north of the Alps, where a larger fraction of more efficient wood burners (e.g., pellet and wood chip burners) is used compared to the South where wood stoves seem to be operated at rather poor combustion conditions (Daellenbach et al., 2017; Zotter et al., 2014). K originating from biomass burning is emitted as KCl (young smoke), and it is then transformed to K_2SO_4 and KNO_3 (aged smoke), which are more stable forms (Niemi et al., 2004). The relatively low S/K ratio observed here (~0.4) is close to the values described in the literature and evidence that the biomass burning aerosols that are detected are relatively freshly emitted (Viana et al., 2013). The diurnal variation of the source contribution reveals that the highest contributions are recorded in the evening hours. Biomass burning contributes 7.2% to PM_{el} on a yearly average, while the contributions are mainly enhanced during the cold period of the year (12.1% cold, 3.1% warm). Contributions during the warm season are mainly attributed to local emissions from public fire and barbecue places close to the measurement site (Herich et al., 2011). Due to this, we assume that this factor is affected by cooking (barbecuing), mainly during the warm season of the year, but since there were restaurants in close proximity to the sampling site, influence during the cold season cannot be excluded as well. Elements in the fine fraction comprise 94% of source profiles' mass, as expected from a combustion process. The factor presents a moderate (~0.6) correlation with TC, OC, and NO_2, and a high correlation (R~0.8) with CO.

3.2.3. *Construction*

This factor accounts for a major fraction of Ca_f (70%), Ca_c (13%), and S_c (14%) and represents construction and the mechanical wear of structures such as pavements and buildings. Calcium is a common constituent of soils and is used for construction materials and as a filler in road surfacing materials (Limbeck et al., 2009). Sulfur in this factor profile and the moderate correlation between S_c and Ca also suggest construction activity, e.g., gypsum ($CaSO_4$). A factor rich in Ca is often found in residential areas, and it is sometimes referred to as city or urban dust (Almeida et al., 2020). Two maxima are recorded during the day at 07:00 and 13:00 (local time), which might indicate the start of the morning shift in the construction sites and the after lunch break shift. The average contribution of the source to PM_{el} is 4.3%, and is higher

during the warm season (5.2% warm, 2.9% cold), probably due to enhanced resuspension under dry conditions, while it retains a 5.2% contribution during the Covid-19 lockdown period. The factor is mainly contributing to the coarse fraction, with the contribution of the coarse elements to the mass of the factor being 66%. No correlation of this factor with external data is observed.

3.2.4. Heavy oil combustion

This factor is characterized by high contributions to Al_f (53%), V_f (48%), Ni_f (31%), Se_f (53%), Br_f (79%), Sn_f (51%), Sb_f (54%), V_c (43%), As_c (26%), Se_c (53%), Rb_c (36%), Sn_c (53%), and Sb_c (54%), and corresponds to heavy oil combustion processes. Ni and V are known as tracers of heavy oil combustion (Maenhaut et al., 2016). Industrial boilers and electricity generation boilers consuming heavy oil are regarded as one of the main sources of such particulates (Jang et al., 2007). Other tracers in the factor correspond to other industrial emissions from the same units. This source might be transported to Zurich, which is reflected by the "flat" diurnal variation and the relatively spiky time series (Fig.S.12.). The average yearly contribution of the source to PM_{el} is 3.3%, and is relatively stable (±0.4%) throughout the year, as is often the case for industry-related activities. This source produces mainly fine particles (75%). The contributions present low correlations (R~0.45) to SO_4^{-2} and the total organics of the ACSM.

3.2.5. Traffic-related factors

Traffic-related emissions are represented by two distinct factors that together account for the largest fraction of Cr_f (71%), Mn_f (35%), Fe_f (62%), Ni_f (50%), Cu_f (60%), Zr_f (38%), and Ba_f (20%), and Cr_c (72%), Ni_c (46%), Fe_c (63%), Cu_c (92%), Zn_c (70%), Zr_c (53%), and Ba_c (53%). An important question here is why two factors are required to describe traffic. Even though both sources have similar tracers, the main difference is that one contains mainly fine elements (85% of the factor's mass) and the other coarse (90% of the factor's mass). In their study in Zürich (Bukowiecki et al., 2009), showed that brake wear particles from light-duty vehicles were distributed in the entire size range larger than 1 μm, while more than 75% of the brake wear emissions from heavy-duty vehicles were found in the coarse mode (10–2.5 μm). According to the same study, the reason behind that observation is likely due to the different design and operating conditions of LDV and HDV brake systems. For that reason, one traffic factor is attributed primarily to Light-Duty Vehicles (LDV) and the other primarily to Heavy-Duty Vehicles (HDV), and the factors are named accordingly. All of those elements in the two factors are well-known tracers of traffic-related emissions (Schauer et al., 2006). Zn, Mn, and Cu are found in brake wear emissions and some tailpipe emissions (Cadle et al., 1999; Schauer et al., 2006). Ba, a major component of many brake pad formulations, and Cr are found in higher concentrations in urban soil and paved road dust compared to crustal composition (Amato et al., 2011; Ho et al., 2003). Zn is also a component of the tires with a relatively high concentration (1%) (Gehrig et al., 2010). Finally, Zr and Fe have been linked to brake wear dust in urban environments (Moreno et al., 2013). The diurnal profiles of the source contributions present the characteristic morning and evening traffic rush hour peaks, but HDV have a much more prominent peak in the morning while LDV in the evening. The contributions of LDV and HDV to PM_{el} are 5.4% and 17%, respectively. In a previous study that took place in Zürich, it was estimated that HDV traffic-related PM_{10} emissions were 6–20 times higher per vehicle compared to LDV (Bukowiecki et al., 2010). The contribution of LDV to PM_{el} is relatively stable during the different seasons (±0.7%), while it decreases significantly during the Covid-19 lockdown period (3.1%). The contribution of HDV to PM_{el} increases during the cold season (19.8%), most likely due to the higher tire and brake wear emissions attributed to winter tires (Ducret-Stich et al., 2013) and reduced dilution. The contribution during the Covid-19 lockdown period decreased to 10%. Both factors have good correlation (R~0.8) with BC and (R~0.7) NO_x.

3.2.6. Industrial emissions

Two industrial emission-related sources were identified and are traced by Pb_f (95%) and Zn_f (60%), respectively. This source was previously identified in Switzerland as a combined Pb and Zn source (Rai et al., 2019). In this study, Zn and Pb are apportioned to separate factors, indicating two different emission sources. This observation is supported by the fact that Zn and Pb time series are not correlated. Source profiles containing Zn and/or Pb have been previously identified but have not been linked to any specific industrial activities (Crilley et al., 2017; Rai et al., 2019; Richard et al., 2011). Both elements are often linked to traffic-related emissions, either due to tire wear for Zn, or fuel and motor oil combustion, brake wear, and resuspension of enriched road dust for Pb (Schauer et al., 2006). The link of those two sources to traffic is not considered in this study for several reasons. Neither the sources, nor the Pb and Zn time series, have the distinct bimodal pattern with traffic rush hour peaks of traffic-related components. Additionally, the source contributions are not correlated with either NOx or BC_{ff}. Earlier studies in Switzerland pointed out that even though during 1998/1999 gradually decreasing concentrations of Pb in PM_{10} from urban traffic sites to the urban background, suburban and rural sites were observed (Hueglin et al., 2005), later studies indicated that Pb had similar concentrations at the different site types (Gianini et al., 2012b). This suggests either spatially uniform sources or long-range transport. Bukowiecki et al. (2009) in their study in Switzerland, also suggested that even though Zn and Pb are linked to traffic in the fine mode, this most likely does not apply in the coarse mode. The link between Pb and traffic is the enrichment of road dust with Pb tailpipe emissions before the phaseout of leaded gasoline (Schauer et al., 2006). This effect should fade out with time, and this might explain why Pb presents similar concentrations at different sites around Switzerland in more recent studies. It has been proposed that the combustion of municipal waste produces submicron particles composed of Zn, Pb, and Cl as well as numerous other metals (Moffet et al., 2008). In Switzerland, many kinds of waste are separately collected and recycled to a large extent. The residual amount of municipal solid waste (MSW) has to be thermally treated before final disposal (Morf et al., 2013). According to data from the Swiss Federal Office of Energy, in 2017, Switzerland had 30 municipal waste incineration plants (MWI), each with a capacity of between 30,000 and 230,000 tonnes per year (Fig. S.15). Additionally, bottom ash produced by MWI, is then recycled by thermo-recycling plants to recycle ferrous and non-ferrous metals in the form of marketable products, some of which have a high content of Zn and Pb (Mehr et al., 2021). The diurnals of both sources show a maximum at early morning hours, most likely due to the shallow boundary layer height. Both sources have very low contribution to PM_{el} (0.7%), which is stable in all seasons and during Covid-19 lockdown.

3.2.7. Mineral dust-related factors

Two factors are related to mineral dust and explain the variation of Si_c (65%), K_c (29%), Ca_c (76%), and Ti_c (49%), and Si_f (98%), Ti_f (62%), Al_c (25%), Si_c (36%), Ti_c (32%), and V_c (19%). These elements are common tracers of mineral dust (Nava et al., 2012; Vasilatou et al., 2017). The sources are differentiated into long-range (transported dust) and short-range (mineral dust). Dust transportation from arid African regions to Europe, often referred to as Saharan Dust events, are very frequent, mainly in Southern Europe (Cesari et al., 2016; Manousakas et al., 2015; Rodriguez et al., 2001), but also in Central Europe and Switzerland (Coen et al., 2004; Ducret-Stich et al., 2013; Flentje et al., 2015; Gianini et al., 2012b). The contribution of mineral dust peaks during the morning rush hour, indicating dust resuspension caused or enhanced by vehicular movement, and in the early afternoon which might be an effect of the increased wind speed during that time that favors resuspension. The average diurnal variation of wind speed for the entire study period is presented in Fig. S.18. in the supporting material. On the other hand, transported dust has low diurnal variation, and additionally, the time series of the contributions are expressed by a

small number of high-intensity pollution events, indicative of Sahara Dust events. The average yearly contribution to PM_{el} is 22.1% and 9.5% for mineral dust and transported dust, respectively. During the dust transport event days the factor has a very high contribution, which is also the highest compared to all other sources (Fig. S.19.). No correlation with the external data is found. Both sources emit coarse particles (mineral dust 96%, transported dust 70%).

3.2.8. Sulfates

This factor is characterized by S_f (88%), and it corresponds to the secondary SO_4^{-2}, which is formed by the oxidation of its precursor gaseous SO_2 (Zhuang et al., 1999). As secondary tracers/components, the factor also explains the variation of As_f (22%) and Se_f (29%). This source has been previously identified in many source apportionment studies in Switzerland and abroad (Gianini et al., 2012a, 2012b; Manousakas et al., 2020; Viana et al., 2008). As and Se are also present in the factor and commonly taken to be tracers of coal combustion (Vejahati et al., 2010), which may indicate long-range transport from other regions in central Europe where coal is mainly used for domestic heating (Almeida et al., 2020). The source contributes 15.4% to PM_{el}, and the contribution is slightly higher during the warm season due to the increased photochemical activity (17.7% warm, 13.1% cold). As expected, the source has a high correlation (R~0.8) to SO_4^{-2} from the ACSM, and 95% of the factor's mass is attributed to the fine tracers.

3.2.9. Railway

This factor contributes to Mn_c (90%) and Fe_c (21%). Particles derived from steel wheels and rails contain a characteristic trace element chemistry and are traced by Mn and Fe (Moreno et al., 2014). The Mn/Fe ratio in the factor is 0.03, relatively close to a Mn/Fe ratio of 0.01, which is consistent with an origin from steel used in wheels, rails, and brakes (Abbasi et al., 2012). Based on abrasive mass losses of wheels, brakes, and tracks, the emissions of PM_{10} from railway traffic were estimated some years ago, to account for 2800 t $year^{-1}$ in Switzerland (Gehrig et al., 2007). Zürich has the busiest railway station in Switzerland, with over 2000 passenger trains scheduled per day. Emissions near big stations, where trains are slowing down or accelerating and passing over track switches, are higher than on open track. Gehrig et al. (2007), found that the railway-induced contribution to ambient PM decreased rapidly with increasing distance from the tracks. This source has also been identified at other Swiss sites (Ducret-Stich et al., 2013). The diurnal variation profile of the source has two peaks at 07:00 and 22:00, as well as a smaller peak at 01:00. The last peak might represent the trains moving back into parking position after the end of the shift and/or cargo trains moving during the night. Additionally, the polar plot of wind direction and speed to the factor contributions indicates that the source is mainly affected by winds from NW direction (Fig. S.16.), which is in agreement with the train station's location. The source has a stable contribution during all seasons (6.6% ± 0.3%), and the factor is comprised mainly of elements in the coarse fraction (80%). It has a good correlation to NO_x (R~0.7). This can be explained either by some mixing of this factor to traffic due to the common tracers of the sources, or to resuspension of deposited railway emitted dust on road surfaces, or random correlation due to similar rush hours of trains and traffic.

3.2.10. Fireworks

This factor contributes to K (17%), Ti (11%), Cu (11%), Sr (76%), Ba (68%), Bi (100%), Sr_c (22%), Bi_c (100%). Although the factor contributes a relatively low percentage of the overall concentration of S and Cl at the site (8% and 17%), they comprise 55% of the total mass of the factor. All of those elements are well-known tracers of fireworks (Kong et al., 2015; Moreno et al., 2007b; Rai et al., 2019; Tanda et al., 2019; Vecchi et al., 2008). In fireworks, metals (such as Mg, Al, Ti, Fe, Zn) are used as pyrotechnic fuels combined with metalloids (Si and B) and non-metals (e.g., charcoal, sulfur); nitrates and chlorates with alkali metal (Na, K) or alkaline earth metal (Ba, Sr) cations or ammonium ions are used as oxidizers (Moreno et al., 2007a; Tanda et al., 2019; Tremper et al., 2018); metal salts of Na, Sr, Ba, Cu, Mg, and Ti are used as colorants; Bi compounds (Bi_2O_3 and $(BiO)_2CO_3$) are commonly used to produce crackling stars as a non-toxic substitute of Pb containing compounds that were used in the past (Tanda et al., 2019). The ratio K/S in the factor equals 2.74, which is in excellent agreement with the elemental concentration ratio of K and S in black powder (2.76) (Dutcher et al., 1999), while the Ba/K ratio of 0.055 is also in good agreement with the proposed ratio of 0.057 (Pongpiachan et al., 2018). Since the composition of fireworks is different according to their type, it is possible that their chemical fingerprint could vary in different areas. Fireworks are detected during Zürich Fest (July 5th, 2019), Swiss National Day celebrations (August 1st, 2019), and New Year's Eve (January 1st, 2020). All other days/time points were constrained to zero. As discussed in the PMF section, firework events were identified by examining the time series of Bi, and K. Fine elements consist of 80% of the mass of the factors, which is in agreement with studies estimating that emitted elements during firework events are mainly in the accumulation mode (Tanda et al., 2019). The diurnal variation of the factor showed a maximum at 23:00, followed by a sharp decrease starting at 01:00 and reaching zero at 04:00. This source, even though it contributes to PM_{el} levels in the area only for a small number of days, owing to the extreme mass contributions on those events (reaching up to 28.9 μg m^{-3}) contributes 2.4% on a yearly average. During the firework event days the factor has the highest contribution compared to all other sources (Fig. S.19.).

3.3. Geographical origins of sources

The plotted backward trajectories (BWT) that correspond to the study period, as well as the most frequent trajectory pathways, are presented in detail in the supporting material. The air pathways are distributed around the sampling site (as an average for the entire sampling period) relatively homogeneously, with the transportation from the South being somewhat less frequent, most likely due to the Alps. All sources were examined for possible effects of long-range transportation, and two were identified to be indeed affected. The CWTs for those two sources are presented in Fig. 8.

The Atlantic Ocean is the source location of salt. Sea salt particles are formed via a bubble-bursting process typically resulting from whitecap generation (de Leeuw et al., 2000). The formed particles are coarse and are usually deposited in coastal regions. Long-range transport of sea salt occurs when local circulations change the vertical distributions of PM, lifting aerosol from the planetary boundary layer into the free troposphere (Chen et al., 2016). Transportation from the Atlantic is favored in this case over the closer located Mediterranean sea, most likely for two reasons. Air masses from the West reach the sampling site easier than from the South due to the Alps, and Switzerland's location in the west wind drift zone. Additionally, above the Atlantic, higher sea salt concentrations are reached than above the Mediterranean due to higher wind speeds (Manders et al., 2010).

Transported dust originates from the Mediterranean and South Europe region, clearly indicating dust transport events. Other sources such as Industry and Sulfates, even though they are expected to be transported, do not present very specific spatial origin, and their CWTs resemble the general wind fingerprint (Fig. S.17.).

4. Conclusions

This study aimed at identifying the PM sources in Zürich, Switzerland, using size segregated elemental composition data using an Xact 625i equipped with a sampling changing inlet, which allowed for alternating sampling of PM_{10} and $PM_{2.5}$. The data were first made continuous by an interpolation. The uncertainty of the interpolated points was then estimated by comparing the $PM_{2.5}/PM_{10}$ of each point to the average $PM_{2.5}/PM_{10}$ of the time series. Using a combination of $PM_{2.5}$

and PM_{coarse} was the best approach for source apportionment using switching inlet data.

Thirteen (13) PM elemental content sources were identified. The sources were namely sea salt (5.4%), biomass burning (7.2%), construction (4.3%), industrial (3.3%), LDV (5.4%), Pb (0.7%), Zn (0.7%), dust (22.1%), transported dust (9.5%), sulfates (15.4%), HDV (17%), railway (6.6%) and fireworks (2.4%). A two-step source apportionment approach was used to get good results when firework data points were included in the analysis. This approach can be used in situations where the data contain high-intensity events that disproportionally affect the PMF solution. Such events contain valuable information and should not be discarded.

The combination of the inlet switching system and the SA approach described in this publication yielded improved PMF results. A clear advantage of this approach is that the model, additionally to the diurnal and seasonal variation of the dataset, also utilizes the variation from the size segregated data, which leads to the identification of more sources. Even though high-intensity events in the dataset add interest to the data, they are known to affect disproportionally the PMF solutions. The methodology proposed in this study has significant advantages over more conventional approaches when treating such data, but it still needs to be tested with long-term datasets from other areas with more frequent pollution events. In such cases, the number of points that are not accurately calculated by the interpolation procedure will increase significantly, and even if high uncertainty is assigned to those points, SA results may not accurately reproduce the situation in the study area.

CRediT authorship contribution statement

M. Manousakas: Conceptualization, Methodology, Validation, Formal analysis, Investigation, Writing – original draft, Visualization. **M. Furger:** Supervision, Investigation, Writing – review & editing, Project administration, Formal analysis, Visualization. **K. Daellenbach:** Supervision, Validation, Writing – review & editing. **F. Canonaco:** Methodology, Software, Writing – review & editing. **G. Chen:** Investigation, Writing – review & editing. **A. Tobler:** Software, Writing – review & editing. **P. Rai:** Investigation. **L. Qi:** Investigation. **A.H. Tremper:** Writing – review & editing. **D. Green:** Writing – review & editing. **C. Hueglin:** Writing – review & editing. **J.G. Slowik:** Writing – review & editing. **I. El Haddad:** Writing – review & editing. **A.S.H. Prevot:** Conceptualization, Writing – review & editing, Supervision, Project administration, Funding acquisition.

Declaration of competing interest

The authors declare that they have no known competing financial interests or personal relationships that could have appeared to influence the work reported in this paper.

Acknowledgments

This study was supported by the Swiss Federal Office of the Environment (FOEN) and the SDC Clean-Air-China Programme (grant number 7F-09802.01.03). We would like to thank Empa/NABEL for technical support and resources. K.R.D. acknowledges support by the SNSF Ambizione grant PZPGP2_201992. We extend our gratitude to the Office for Real Estates Zurich (Immobilienamt) for providing permission to park the trailer for one year in this place and to the immediate neighbors in the Zeughaush of for their patience. We thank Günther Wehrle, René Richter, Pascal Schneider, and Ivo Beck of PSI for their help in setting up and maintaining the station.

Appendix A. Supplementary data

Supplementary data to this article can be found online at https://doi.org/10.1016/j.aeaoa.2022.100165.

References

Abbasi, S., Olander, L., Larsson, C., Olofsson, U., Jansson, A., Sellgren, U., 2012. A field test study of airborne wear particles from a running regional train. Proc. Inst. Mech. Eng. - Part F J. Rail Rapid Transit 226, 95–109. https://doi.org/10.1177/0954409711408774.

Almeida, S.M., Manousakas, M., Diapouli, E., Kertesz, Z., Samek, L., Hristova, E., Sega, K., Alvarez, R.P., Belis, C.A., Eleftheriadis, K., Group, he I.E.R.S, 2020. Ambient particulate matter source apportionment using receptor modelling in European and Central Asia urban areas. Environ. Pollut. 266, 115199. https://doi.org/10.1016/j.envpol.2020.115199.

Amato, F., Alastuey, A., Karanasiou, A., Lucarelli, F., Nava, S., Calzolai, G., Severi, M., Becagli, S., Gianelle, V.L., Colombi, C., Alves, C., Custódio, D., Nunes, T., Cerqueira, M., Pio, C., Eleftheriadis, K., Diapouli, E., Reche, C., Minguillón, C., Manousakas, M., Maggos, T., Vratolis, S., Harrison, R.M., Querol, X., 2016. AIRUSE-LIFE + : a harmonized PM speciation and source apportionment in five southern European cities. Atmos. Chem. Phys. 16, 3289–3309. https://doi.org/10.5194/acp-16-3289-2016.

Amato, F., Hopke, P.K., 2012. Source apportionment of the ambient PM2.5 across St. Louis using constrained positive matrix factorization. Atmos. Environ. 46, 329–337. https://doi.org/10.1016/j.atmosenv.2011.09.062.

Amato, F., Pandolfi, M., Moreno, T., Furger, M., Pey, J., Alastuey, A., Bukowiecki, N., Prevot, A.S.H., Baltensperger, U., Querol, X., 2011. Sources and variability of inhalable road dust particles in three European cities. Atmos. Environ. 45, 6777–6787. https://doi.org/10.1016/j.atmosenv.2011.06.003.

Angyal, A., Ferenczi, Z., Manousakas, M., Furu, E., Szoboszlai, Z., Török, Z., 2021. Source identification of fine and coarse aerosol during smog episodes in Debrecen , Hungary. Air Qual. Atmos. Heal. https://doi.org/10.1007/s11869-021-01008-8.

Annegarn, H.J., Flanz, M., Kenntner, T., Kneen, M.A., Helas, G., Piketh, S.J., 1996. Airborne streaker sampling for PIXE analysis. Nucl. Instruments Methods Phys. Res. Sect. B Beam Interact. with Mater. Atoms 109–110, 548–550. https://doi.org/10.1016/0168-583X(95)00966-3.

Belis, C.A., Karagulian, F., Amato, F., Almeida, M., Artaxo, P., Beddows, D.C.S., Bernardoni, V., Bove, M.C., Carbone, S., Cesari, D., Contini, D., Cuccia, E., Diapouli, E., Eleftheriadis, K., Favez, O., El Haddad, I., Harrison, R.M., Hellebust, S., Hovorka, J., Jang, E., Jorquera, H., Kammermeier, T., Karl, M., Lucarelli, F., Mooibroek, D., Nava, S., Nøjgaard, J.K., Paatero, P., Pandolfi, M., Perrone, M.G., Petit, J.E., Pietrodangelo, A., Pokorná, P., Prati, P., Prevot, A.S.H., Quass, U., Querol, X., Saraga, D., Sciare, J., Sfetsos, A., Valli, G., Vecchi, R., Vestenius, M., Yubero, E., Hopke, P.K., 2015. A new methodology to assess the performance and uncertainty of source apportionment models II: the results of two European intercomparison exercises. Atmos. Environ. 123, 240–250. https://doi.org/10.1016/j.atmosenv.2015.10.068.

Brown, S.G., Eberly, S., Paatero, P., Norris, G.a., 2015. Methods for estimating uncertainty in PMF solutions: examples with ambient air and water quality data and guidance on reporting PMF results. Sci. Total Environ. 518–519. https://doi.org/10.1016/j.scitotenv.2015.01.022, 1–10.

Bukowiecki, N., Gehrig, R., Hill, M., Lienemann, P., Zwicky, C.N., Buchmann, B., Weingartner, E., Baltensperger, U., 2007. Iron, manganese and copper emitted by cargo and passenger trains in Zürich (Switzerland): size-segregated mass concentrations in ambient air. Atmos. Environ. 41, 878–889. https://doi.org/10.1016/j.atmosenv.2006.07.045.

Bukowiecki, N., Lienemann, P., Hill, M., Figi, R., Richard, A., Furger, M., Rickers, K., Falkenberg, G., Zhao, Y., Cliff, S.S., Prevot, A.S.H., Baltensperger, U., Buchmann, B., Gehrig, R., 2009. Real-world emission factors for antimony and other brake wear related trace elements: size-segregated values for light and heavy duty vehicles. Environ. Sci. Technol. 43, 8072–8078. https://doi.org/10.1021/es9006096.

Bukowiecki, N., Lienemann, P., Hill, M., Furger, M., Richard, A., Amato, F., Prévôt, A.S.H., Baltensperger, U., Buchmann, B., Gehrig, R., 2010. PM10 emission factors for non-exhaust particles generated by road traffic in an urban street canyon and along a freeway in Switzerland. Atmos. Environ. 44, 2330–2340. https://doi.org/10.1016/j.atmosenv.2010.03.039.

Cadle, S.H., Mulawa, P.A., Hunsanger, E.C., Nelson, K., Ragazzi, R.A., Barrett, R., Gallagher, G.L., Lawson, D.R., Knapp, K.T., Snow, R., 1999. Composition of light-duty motor vehicle exhaust particulate matter in the Denver, Colorado area. Environ. Sci. Technol. 33, 2328–2339. https://doi.org/10.1021/es9810843.

Canonaco, F., Crippa, M., Slowik, J.G., Baltensperger, U., Prévôt, A.S.H., 2013. SoFi, an IGOR-based interface for the efficient use of the generalized multilinear engine (ME-2) for the source apportionment: ME-2 application to aerosol mass spectrometer data. Atmos. Meas. Tech. 6, 3649–3661. https://doi.org/10.5194/amt-6-3649-2013.

Canonaco, F., Slowik, J.G., Baltensperger, U., Prévôt, A.S.H., 2015. Seasonal differences in oxygenated organic aerosol composition: implications for emissions sources and factor analysis. Atmos. Chem. Phys. 15, 6993–7002. https://doi.org/10.5194/acp-15-6993-2015.

Canonaco, F., Tobler, A., Chen, G., Sosedova, Y., Slowik, J.G., Bozzetti, C., Daellenbach, K.R., El Haddad, I., Crippa, M., Huang, R.-J., Furger, M., Baltensperger, U., Prévôt, A.S.H., 2021. A new method for long-term source apportionment with time-dependent factor profiles and uncertainty assessment using SoFi Pro: application to 1 year of organic aerosol data. Atmos. Meas. Tech. 14, 923–943. https://doi.org/10.5194/amt-14-923-2021.

Carslaw, D.C., Ropkins, K., 2012. Openair - an r package for air quality data analysis. Environ. Model. Software 27 (28), 52–61. https://doi.org/10.1016/j.envsoft.2011.09.008.

Cesari, D., Donateo, A., Conte, M., Merico, E., Giangreco, A., Giangreco, F., Contini, D., 2016. An inter-comparison of PM2.5 at urban and urban background sites: chemical

characterization and source apportionment. Atmos. Res. 174–175, 106–119. https://doi.org/10.1016/j.atmosres.2016.02.004.
Chen, Y., Cheng, Y., Ma, N., Wolke, R., Nordmann, S., Schüttauf, S., Ran, L., Wehner, B., Birmili, W., Van Der Gon, H.A.C.D., Mu, Q., Barthel, S., Spindler, G., Stieger, B., Müller, K., Zheng, G.J., Pöschl, U., Su, H., Wiedensohler, A., 2016. Sea salt emission, transport and influence on size-segregated nitrate simulation: a case study in northwestern Europe by WRF-Chem. Atmos. Chem. Phys. 16, 12081–12097. https://doi.org/10.5194/acp-16-12081-2016.
Coen, M.C., Weingartner, E., Schaub, D., Hueglin, C., Corrigan, C., Henning, S., Schwikowski, M., 2004. Saharan dust events at the Jungfraujoch dtection by wavelength deenden of the single scattering albedo and first climatology analysis. Atmos. Chem. Phys. 4, 2465–2480. https://doi.org/10.5194/acp-4-2465-2004.
Crilley, L.R., Lucarelli, F., Bloss, W.J., Harrison, R.M., Beddows, D.C., Calzolai, G., Nava, S., Valli, G., Bernardoni, V., Vecchi, R., 2017. Source apportionment of fine and coarse particles at a roadside and urban background site in London during the 2012 summer ClearfLo campaign. Environ. Pollut. 220, 766–778. https://doi.org/10.1016/j.envpol.2016.06.002.
Crippa, M., Canonaco, F., Lanz, V.A., Äijälä, M., Allan, J.D., Carbone, S., Capes, G., Ceburnis, D., Dall'Osto, M., Day, D.A., DeCarlo, P.F., Ehn, M., Eriksson, A., Freney, E., Hildebrandt, L.R., Hillamo, R., Jimenez, J.L., Junninen, H., Kiendler-Scharr, A., Kortelainen, A.-M., Kulmala, M., Laaksonen, A., Mensah, A.A., Mohr1, C., Nemitz, E., O'Dowd, C., Ovadnevaite, J., Pandis, S.N., Petäjä, T., Poulain, L., Saarikoski, S., Sellegri, K., Swietlicki, E., Tiitta, P., Worsnop D, R., Baltensperger, U., Prévôt, A.S.H., 2014. Organic aerosol components derived from 25 AMS data sets across Europe using a consistent ME-2 based source apportionment approach. Atmos. Chem. Phys. 14, 6159–6176. https://doi.org/10.5194/acp-14-6159-2014.
Crippa, M., Decarlo, P.F., Slowik, J.G., Mohr, C., Heringa, M.F., Chirico, R., Poulain, L., Freutel, F., Sciare, J., Cozic, J., Di Marco, C.F., Elsasser, M., Nicolas, J.B., Marchand, N., Abidi, E., Wiedensohler, A., Drewnick, F., Schneider, J., Borrmann, S., Nemitz, E., Zimmermann, R., Jaffrezo, J.L., Prévôt, A.S.H., Baltensperger, U., 2013. Wintertime aerosol chemical composition and source apportionment of the organic fraction in the metropolitan area of Paris. Atmos. Chem. Phys. 13, 961–981. https://doi.org/10.5194/acp-13-961-2013.
Daellenbach, K.R., Bozzetti, C., Křepelová, A., Canonaco, F., Wolf, R., Zotter, P., Fermo, P., Crippa, M., Slowik, J.G., Sosedova, Y., Zhang, Y., Huang, R.J., Poulain, L., Szidat, S., Baltensperger, U., El Haddad, I., Prévôt, A.S.H., 2016. Characterization and source apportionment of organic aerosol using offline aerosol mass spectrometry. Atmos. Meas. Tech. 9, 23–39. https://doi.org/10.5194/amt-9-23-2016.
Daellenbach, K.R., Stefenelli, G., Bozzetti, C., Vlachou, A., Fermo, P., Gonzalez, R., Piazzalunga, A., Colombi, C., Canonaco, F., Hueglin, C., Kasper-Giebl, A., Jaffrezo, J. L., Bianchi, F., Slowik, J.G., Baltensperger, U., El-Haddad, I., Prévôt, A.S.H., 2017. Long-term chemical analysis and organic aerosol source apportionment at nine sites in central Europe: source identification and uncertainty assessment. Atmos. Chem. Phys. 17, 13265–13282. https://doi.org/10.5194/acp-17-13265-2017.
Daellenbach, K.R., Uzu, G., Jiang, J., Cassagnes, L.E., Leni, Z., Vlachou, A., Stefenelli, G., Canonaco, F., Weber, S., Segers, A., Kuenen, J.J.P., Schaap, M., Favez, O., Albinet, A., Aksoyoglu, S., Dommen, J., Baltensperger, U., Geiser, M., El Haddad, I., Jaffrezo, J.L., Prévôt, A.S.H., 2020. Sources of particulate-matter air pollution and its oxidative potential in Europe. Nature 587, 414–419. https://doi.org/10.1038/s41586-020-2902-8.
de Leeuw, G., Neele, F.P., Hill, M., Smith, M.H., Vignati, E., 2000. Production of sea spray aerosol in the surf zone. J. Geophys. Res. 105, 29397. https://doi.org/10.1029/2000JD900549.
Drinovec, L., Močnik, G., Zotter, P., Prévôt, A.S.H., Ruckstuhl, C., Coz, E., Rupakheti, M., Sciare, J., Müller, T., Wiedensohler, A., Hansen, A.D.A., 2015. The "dual-spot" Aethalometer: an improved measurement of aerosol black carbon with real-time loading compensation. Atmos. Meas. Tech. 8, 1965. https://doi.org/10.5194/amt-8-1965-2015, 1979.
Ducret-Stich, R.E., Tsai, M.Y., Thimmaiah, D., Künzli, N., Hopke, P.K., Phuleria, H.C., 2013. PM10 source apportionment in a Swiss Alpine valley impacted by highway traffic. Environ. Sci. Pollut. Res. 20, 6496–6508. https://doi.org/10.1007/s11356-013-1682-1.
Dutcher, D.D., Perry, K.D., Cahill, T.A., Copeland, S.A., 1999. Effects of indoor pyrotechnic displays on the air quality in the houston astrodome. J. Air Waste Manag. Assoc. 49, 156–160. https://doi.org/10.1080/10473289.1999.10463790.
EC, 1999. Directive 1999/30 - Limit values for sulphur dioxide, nitrogen dioxide and oxides of nitrogen, particulate matter and lead in ambient air.
EC, 2004. Directive 2004/107/EC of the European Parliament and of the Council relating to arsenic, cadmium, mercury, nickel and polycyclic aromatic hydrocarbons in ambient air.
Flentje, H., Briel, B., Beck, C., Collaud Coen, M., Fricke, M., Cyrys, J., Gu, J., Pitz, M., Thomas, W., 2015. Identification and monitoring of Saharan dust: an inventory representative for south Germany since 1997. Atmos. Environ. 109, 87–96. https://doi.org/10.1016/j.atmosenv.2015.02.023.
Forello, A., Bernardoni, V., Calzolai, G., Lucarelli, F., Massabò, D., Nava, S., Pileci, R., Prati, P., Valentini, S., Valli, G., Vecchi, R., 2019. Exploiting multi-wavelength aerosol absorption coefficients in a multi-time source apportionment study to retrieve source-dependent absorption parameters. Atmos. Chem. Phys. 1–26. https://doi.org/10.5194/acp-2019-123.
Furger, M., Minguillón, M.C., Yadav, V., Slowik, J.G., Hüglin, C., Fröhlich, R., Petterson, K., Baltensperger, U., Prévôt, A.S.H., 2017. Elemental composition of ambient aerosols measured with high temporal resolution using an online XRF spectrometer. Atmos. Meas. Tech. 10, 2061–2076. https://doi.org/10.5194/amt-10-2061-2017.
Furger, M., Rai, P., Slowik, J.G., Cao, J., Visser, S., Baltensperger, U., Prévôt, A.S.H., 2020. Automated alternating sampling of PM10 and PM2.5 with an online XRF spectrometer. Atmos. Environ. X 5. https://doi.org/10.1016/j.aeaoa.2020.100065.
Gehrig, R., Hill, M., Lienemann, P., Zwicky, C.N., Bukowiecki, N., Weingartner, E., Baltensperger, U., Buchmann, B., 2007. Contribution of railway traffic to local PM10 concentrations in Switzerland. Atmos. Environ. 41, 923–933. https://doi.org/10.1016/j.atmosenv.2006.09.021.
Gehrig, R., Zeyer, K., Bukowiecki, N., Lienemann, P., Poulikakos, L.D., Furger, M., Buchmann, B., 2010. Mobile load simulators - a tool to distinguish between the emissions due to abrasion and resuspension of PM10 from road surfaces. Atmos. Environ. 44, 4937–4943. https://doi.org/10.1016/j.atmosenv.2010.08.020.
Gianini, M.F.D., Fischer, A., Gehrig, R., Ulrich, A., Wichser, A., Piot, C., Besombes, J.L., Hueglin, C., 2012a. Comparative source apportionment of PM10 in Switzerland for 2008/2009 and 1998/1999 by positive matrix factorisation. Atmos. Environ. 54, 149–158. https://doi.org/10.1016/j.atmosenv.2012.02.036.
Gianini, M.F.D., Gehrig, R., Fischer, A., Ulrich, A., Wichser, A., Hueglin, C., 2012b. Chemical composition of PM10 in Switzerland: an analysis for 2008/2009 and changes since 1998/1999. Atmos. Environ. Times 54, 97–106. https://doi.org/10.1016/j.atmosenv.2012.02.037.
Hallquist, M., Wenger, J.C., Baltensperger, U., Rudich, Y., Simpson, D., Claeys, M., Dommen, J., Donahue, N.M., George, C., Goldstein, A.H., Hamilton, J.F., Herrmann, H., Hoffmann, T., Iinuma, Y., Jang, M., Jenkin, M.E., Jimenez, J.L., Kiendler-Scharr, A., Maenhaut, W., McFiggans, G., Mentel, T.F., Monod, A., Prévôt, A.S.H., Seinfeld, J.H., Surratt, J.D., Szmigielski, R., Wildt, J., 2009. The formation, properties and impact of secondary organic aerosol: current and emerging issues. Atmos. Chem. Phys. 9, 5155–5236. https://doi.org/10.5194/acp-9-5155-2009.
Hasheminassab, S., Sowlat, M.H., Pakbin, P., Katzenstein, A., Low, J., Polidori, A., 2020. High time-resolution and time-integrated measurements of particulate metals and elements in an environmental justice community within the Los Angeles Basin: spatio-temporal trends and source apportionment. Atmos. Environ. X 7, 100089. https://doi.org/10.1016/j.aeaoa.2020.100089.
Heo, J.B., Hopke, P.K., Yi, S.M., 2009. Source apportionment of PM2.5 in seoul, korea. Atmos. Chem. Phys. 9, 4957–4971. https://doi.org/10.5194/acp-9-4957-2009.
Herich, H., Hueglin, C., Buchmann, B., 2011. A 2.5 year's source apportionment study of black carbon from wood burning and fossil fuel combustion at urban and rural sites in Switzerland. Atmos. Meas. Tech. 4, 1409–1420. https://doi.org/10.5194/amt-4-1409-2011.
Ho, K.F., Lee, S.C., Chow, J.C., Watson, J.G., 2003. Characterization of PM10 and PM2.5 source profiles for fugitive dust in Hong Kong. Atmos. Environ. 37, 1023–1032. https://doi.org/10.1016/S1352-2310(02)01028-2.
Hueglin, C., Gehrig, R., Baltensperger, U., Gysel, M., Monn, C., Vonmont, H., 2005. Chemical characterisation of PM2.5, PM10 and coarse particles at urban, near-city and rural sites in Switzerland. Atmos. Environ. 39, 637–651. https://doi.org/10.1016/j.atmosenv.2004.10.027.
Jang, H.N., Seo, Y.C., Lee, J.H., Hwang, K.W., Yoo, J.I., Sok, C.H., Kim, S.H., 2007. Formation of fine particles enriched by V and Ni from heavy oil combustion: anthropogenic sources and drop-tube furnace experiments. Atmos. Environ. 41, 1053–1063. https://doi.org/10.1016/j.atmosenv.2006.09.011.
Jayarathne, T., Stockwell, C.E., Christian, T.J., Bhave, P.V., Praveen, P.S., Panday, A.K., Adhikari, S., Maharjan, R., Goetz, J.D., DeCarlo, P.F., Saikawa, E., Yokelson, R.J., Stone, E.A., 2017. Nepal Ambient Monitoring and Source Testing Experiment (NAMaSTE): Emissions of Particulate Matter from Wood and Dung Cooking Fires, Brick Kilns, Generators, Trash and Crop Residue Burning. Submitted 2259–2286.
Kim, E., Hopke, P.K., Edgerton, E.S., 2003. Source identification of atlanta aerosol by positive matrix factorization. J. Air Waste Manag. Assoc. 53, 731–739. https://doi.org/10.1080/10473289.2003.10466209.
Kong, S.F., Li, L., Li, X.X., Yin, Y., Chen, K., Liu, D.T., Yuan, L., Zhang, Y.J., Shan, Y.P., Ji, Y.Q., 2015. The impacts of firework burning at the Chinese Spring Festival on air quality: insights of tracers, source evolution and aging processes. Atmos. Chem. Phys. 15, 2167–2184. https://doi.org/10.5194/acp-15-2167-2015.
Lanz, V.A., Hueglin, C., Buchmann, B., Hill, M., Locher, R., Staehelin, J., Reimann, S., 2008. Receptor modeling of C2-C7 hydrocarbon sources at an urban background site in Zurich, Switzerland: changes between 1993-1994 and 2005-2006. Atmos. Chem. Phys. 8, 2313–2332. https://doi.org/10.5194/acp-8-2313-2008.
Limbeck, A., Handler, M., Puls, C., Zbiral, J., Bauer, H., Puxbaum, H., 2009. Impact of mineral components and selected trace metals on ambient PM10 concentrations. Atmos. Environ. 43, 530–538. https://doi.org/10.1016/j.atmosenv.2008.10.012.
Liu, Y., Zheng, M., Yu, M., Cai, X., Du, H., Li, J., Zhou, T., Yan, C., Wang, X., Shi, Z., Harrison, R.M., Zhang, Q., He, K., 2019. High-time-resolution source apportionment of PM2.5 in Beijing with multiple models. Atmos. Chem. Phys. 19, 6595–6609. https://doi.org/10.5194/acp-19-6595-2019.
Lucarelli, F., Nava, S., Calzolai, G., Chiari, M., Udisti, R., Marino, F., 2011. Is PIXE still a useful technique for the analysis of atmospheric aerosols? The LABEC experience. X Ray Spectrom. 40, 162–167. https://doi.org/10.1002/xrs.1312.
Maenhaut, W., Vermeylen, R., Claeys, M., Vercauteren, J., Roekens, E., 2016. Sources of the PM10 aerosol in Flanders, Belgium, and re-assessment of the contribution from wood burning. Sci. Total Environ. 562, 550–560. https://doi.org/10.1016/j.scitotenv.2016.04.074.
Manders, A.M.M., Schaap, M., Querol, X., Albert, M.F.M.A., Vercauteren, J., Kuhlbusch, T.A.J., Hoogerbrugge, R., 2010. Sea salt concentrations across the European continent. Atmos. Environ. 44, 2434–2442. https://doi.org/10.1016/j.atmosenv.2010.03.028.
Manousakas, M., Diapouli, E., Belis, C.A., Vasilatou, V., Gini, M., Lucarelli, F., Querol, X., Eleftheriadis, K., 2021. Quantitative Assessment of the variability in chemical profiles from source apportionment analysis of PM10 and PM2.5 at different sites

within a large Metropolitan area. Environ. Res. 192, 110257. https://doi.org/10.1016/j.envres.2020.110257.
Manousakas, M., Diapouli, E., Papaefthymiou, H., Migliori, a., Karydas, a.G., Padilla-Alvarez, R., Bogovac, M., Kaiser, R.B., Jaksic, M., Bogdanovic-Radovic, I., Eleftheriadis, K., 2015. Source apportionment by PMF on elemental concentrations obtained by PIXE analysis of PM10 samples collected at the vicinity of lignite power plants and mines in Megalopolis, Greece. Nucl. Instrum. Methods Phys. Res. Sect. B Beam Interact. Mater. Atoms 349, 114–124. https://doi.org/10.1016/j.nimb.2015.02.037.
Manousakas, M., Papaefthymiou, H., Diapouli, E., Migliori, A., Karydas, A.G., Bogdanovic-Radovic, I., Eleftheriadis, K., 2017. Assessment of PM2.5 sources and their corresponding level of uncertainty in a coastal urban area using EPA PMF 5.0 enhanced diagnostics. Sci. Total Environ. 574, 155–164. https://doi.org/10.1016/j.scitotenv.2016.09.047.
Manousakas, M.I., Florou, K., Pandis, S.N., 2020. Source apportionment of fine organic and inorganic atmospheric aerosol in an urban background area in Greece. Atmosphere 11. https://doi.org/10.3390/atmos11040330.
Massabò, D., Prati, P., 2021. An overview of optical and thermal methods for the characterization of carbonaceous aerosol, La Rivista del Nuovo Cimento. Springer Berlin Heidelberg. https://doi.org/10.1007/s40766-021-00017-8.
Mazzei, F., Lucarelli, F., Nava, S., Prati, P., Valli, G., Vecchi, R., 2007. A new methodological approach: the combined use of two-stage streaker samplers and optical particle counters for the characterization of airborne particulate matter. Atmos. Environ. 41, 5525–5535. https://doi.org/10.1016/j.atmosenv.2007.04.012.
Mcnamara, S.M., Kolesar, K.R., Wang, S., Kirpes, R.M., May, N.W., Gunsch, M.J., Cook, R.D., Fuentes, J.D., Hornbrook, R.S., Apel, E.C., China, S., Laskin, A., Pratt, K. A., 2020. Observation of road salt aerosol driving inland wintertime atmospheric chlorine chemistry. ACS Cent. Sci. 6, 684–694. https://doi.org/10.1021/acscentsci.9b00994.
Mehr, J., Haupt, M., Skutan, S., Morf, L., Raka Adrianto, L., Weibel, G., Hellweg, S., 2021. The environmental performance of enhanced metal recovery from dry municipal solid waste incineration bottom ash. Waste Manag. 119, 330–341. https://doi.org/10.1016/j.wasman.2020.09.001.
MeteoSchweiz 2020a: Klimabulletin Jahr 2019. https://www.meteoschweiz.admin.ch/content/dam/meteoswiss/de/service-und-publikationen/Publikationen/doc/2019_ANN_d.pdf (accessed 2020-10-27).
MeteoSchweiz, 2020b: Klimabülletin Frühling 2020. https://www.meteoschweiz.admin.ch/content/dam/meteoswiss/de/Ungebundene-Seiten/Publikationen/Klimabulletin/doc/klimabulletin_fruehling_2020_d.pdf?=&pageIndex=0&tab=search_tab. (accessed 2020-10-27).
Moffet, R.C., Desyaterik, Y., Hopkins, R.J., Tivanski, A.V., Gilles, M.K., Wang, Y., Shutthanandan, V., Molina, L.T., Abraham, R.G., Johnson, K.S., Mugica, V., Molina, M.J., Laskin, A., Prather, K.A., 2008. Characterization of aerosols containing Zn, Pb, and Cl from an industrial region of Mexico City. Environ. Sci. Technol. 42, 7091–7097. https://doi.org/10.1021/es7030483.
Moreno, T., Alastuey, A., Querol, X., Font, O., Gibbons, W., 2007a. The identification of metallic elements in airborne particulate matter derived from fossil fuels at Puertollano, Spain. Int. J. Coal Geol. 71, 122–128. https://doi.org/10.1016/j.coal.2006.08.001.
Moreno, T., Karanasiou, a., Amato, F., Lucarelli, F., Nava, S., Calzolai, G., Chiari, M., Coz, E., Artíñano, B., Lumbreras, J., Borge, R., Boldo, E., Linares, C., Alastuey, a., Querol, X., Gibbons, W., 2013. Daily and hourly sourcing of metallic and mineral dust in urban air contaminated by traffic and coal-burning emissions. Atmos. Environ. 68, 33–44. https://doi.org/10.1016/j.atmosenv.2012.11.037.
Moreno, T., Martins, V., Querol, X., Jones, T., BéruBé, K., Minguillón, M.C., Amato, F., Capdevila, M., de Miguel, E., Centelles, S., Gibbons, W., 2014. A new look at inhalable metalliferous airborne particles on rail subway platforms. Sci. Total Environ. 505, 367–375. https://doi.org/10.1016/j.scitotenv.2014.10.013.
Moreno, T., Querol, X., Alastuey, A., Cruz Minguillón, M., Pey, J., Rodriguez, S., Vicente Miró, J., Felis, C., Gibbons, W., 2007b. Recreational atmospheric pollution episodes: inhalable metalliferous particles from firework displays. Atmos. Environ. 41, 913–922. https://doi.org/10.1016/j.atmosenv.2006.09.019.
Morf, L.S., Gloor, R., Haag, O., Haupt, M., Skutan, S., Lorenzo, F., Di Böni, D., 2013. Precious metals and rare earth elements in municipal solid waste - sources and fate in a Swiss incineration plant. Waste Manag. 33, 634–644. https://doi.org/10.1016/j.wasman.2012.09.010.
Nava, S., Becagli, S., Calzolai, G., Chiari, M., Lucarelli, F., Prati, P., Traversi, R., Udisti, R., Valli, G., Vecchi, R., 2012. Saharan dust impact in central Italy: an overview on three years elemental data records. Atmos. Environ. 60, 444–452. https://doi.org/10.1016/j.atmosenv.2012.06.064.
Ng, N.L., Herndon, S.C., Trimborn, A., Canagaratna, M.R., Croteau, P.L., Onasch, T.B., Sueper, D., Worsnop, D.R., Zhang, Q., Sun, Y.L., Jayne, J.T., 2011. An Aerosol Chemical Speciation Monitor (ACSM) for routine monitoring of the composition and mass concentrations of ambient aerosol. Aerosol Sci. Technol. 45, 780–794. https://doi.org/10.1080/02786826.2011.560211.
Niemi, J.V., Tervahattu, H., Vehkamäki, H., Kulmala, M., Koskentalo, T., Sillanpää, M., Rantamäki, M., 2004. Characterization and source identification of a fine particle episode in Finland. Atmos. Environ. 38, 5003–5012. https://doi.org/10.1016/j.atmosenv.2004.06.023.
Osto, M.D., Querol, X., Amato, F., Karanasiou, A., Lucarelli, F., Nava, S., Calzolai, G., Chiari, M., 2013. Hourly elemental concentrations in PM 2 . 5 aerosols sampled simultaneously at urban background and road site during SAPUSS Biogeosciences – diurnal variations and PMF receptor modelling. Atmos. Chem. Phys. 13, 4375–4392. https://doi.org/10.5194/acp-13-4375-2013.
Paatero, P., Hopke, P.K., 2003. Discarding or downweighting high-noise variables in factor analytic models. Anal. Chim. Acta 490, 277–289. https://doi.org/10.1016/S0003-2670(02)01643-4.
Paatero, P., Hopke, P.K., Song, X.-H., Ramadan, Z., 2002. Understanding and controlling rotations in factor analytic models. Chemometr. Intell. Lab. Syst. 60, 253–264. https://doi.org/10.1016/S0169-7439(01)00200-3.
Paatero, P., Tappert, U., 1994. Positive Matrix Factorization : a non-negative factor model with optimal utilization of error stimates od data values. Environmetrics 5, 111–126.
Pandis, S.N., Wexler, A.S., Seinfeld, J.H., 1993. Secondary organic aerosol formation a N D T R a N S P O R T - - I I . predicting the ambient secondary organic aerosol size distribution. Atmos. Environ. 27, 2403–2416.
Peré-Trepat, E., Kim, E., Paatero, P., Hopke, P.K., 2007. Source apportionment of time and size resolved ambient particulate matter measured with a rotating DRUM impactor. Atmos. Environ. 41, 5921–5933. https://doi.org/10.1016/j.atmosenv.2007.03.022.
Pey, J., Querol, X., Alastuey, A., Forastiere, F., Stafoggia, M., 2013. African dust outbreaks over the Mediterranean Basin during 2001-2011: PM10 concentrations, phenomenology and trends, and its relation with synoptic and mesoscale meteorology. Atmos. Chem. Phys. 13, 1395–1410. https://doi.org/10.5194/acp-13-1395-2013.
Pokorná, P., Hovorka, J., Hopke, P.K., 2016. Elemental composition and source identification of very fine aerosol particles in a European air pollution hot-spot. Atmos. Pollut. Res. 7, 671–679. https://doi.org/10.1016/j.apr.2016.03.001.
Pokorna, P., Hovorka, J., Klan, M., Hopke, P.K., 2015. Source apportionment of size resolved particulate matter at a European air pollution hot spot. Sci. Total Environ. 502, 172–183. https://doi.org/10.1016/j.scitotenv.2014.09.021.
Polissar, V., Hopke, P.K., Paatero, P., Malm, W.C., Sisler, J.F., 1998. Atmospheric aerosol over Alaska 2 . Elemental composition and sources. J. Geophys. Res. 103, 19045–19057.
Pongpiachan, S., Iijima, A., Cao, J., 2018. Hazard quotients, hazard indexes, and cancer risks of toxic metals in PM10 during firework displays. Atmosphere 9, 1–18. https://doi.org/10.3390/atmos9040144.
Prati, P., Zucchiatti, A., Tonus, S., Lucarelli, F., Mandò, P.A., Ariola, V., 1998. A testing technique of streaker aerosol samplers via PIXE analysis. Nucl. Instruments Methods Phys. Res. Sect. B Beam Interact. with Mater. Atoms 136–138, 986–989. https://doi.org/10.1016/S0168-583X(97)00744-1.
Qi, L., Chen, M., Stefenelli, G., Pospisilova, V., Lopez-Hilfiker, F.D., Daellenbach, K.R., Hüglin, C., Tong, Y., Baltensperger, U., Prevot, A.S.H., Slowik, J.G., 2019. Organic aerosol source apportionment in Zurich using an extractive electrospray ionization time-of-flight mass spectrometer (EESI-TOF-MS) - Part 1: biogenic influences and day-night chemistry in summer. Atmos. Chem. Phys. 19, 14825–14848. https://doi.org/10.5194/acp-19-14825-2019.
Raabe, O.G., Braaten, D.A., Axelbaum, R.L., Teague, S.V., Cahill, T.A., 1988. Calibration studies of the drum impactor. J. Aerosol Sci. 19, 183–195. https://doi.org/10.1016/0021-8502(88)90222-4.
Rai, P., Furger, M., El Haddad, I., Kumar, V., Wang, L., Singh, A., Dixit, K., Bhattu, D., Petit, J.E., Ganguly, D., Rastogi, N., Baltensperger, U., Tripathi, S.N., Slowik, J.G., Prévôt, A.S.H., 2020. Real-time measurement and source apportionment of elements in Delhi's atmosphere. Sci. Total Environ. 742, 140332. https://doi.org/10.1016/j.scitotenv.2020.140332.
Rai, P., Furger, M., Slowik, J., Canonaco, F., Fröhlich, R., Hüglin, C., Minguillón, M.C., Petterson, K., Baltensperger, U., Prévôt, A.S.H., 2019. Source apportionment of highly time resolved trace elements during a firework episode from a rural freeway site in Switzerland. Atmos. Chem. Phys. Discuss. 1–25. https://doi.org/10.5194/acp-2018-1229.
Rai, P., Furger, M., Slowik, J.G., Zhong, H., Tong, Y., Wang, L., Duan, J., Gu, Y., Qi, L., Huang, R.J., Cao, J., Baltensperger, U., Prévôt, A.S.H., 2021a. Characteristics and sources of hourly elements in PM10 and PM2.5 during wintertime in Beijing. Environ. Pollut. 278 https://doi.org/10.1016/j.envpol.2021.116865.
Rai, P., Slowik, J.G., Furger, M., Haddad, I., El Visser, S., Tong, Y., Singh, A., Wehrle, G., Kumar, V., Tobler, A.K., Bhattu, D., Wang, L., 2021b. Highly time-resolved measurements of element concentrations in PM 10 and PM 2 . 5 : comparison of Delhi , Beijing , London , and Krakow. Atmos. Chem. Phys. 21, 717–730.
Reff, A., Eberly, S.I., Bhave, P.V., 2007. Receptor modeling of ambient particulate matter data using positive matrix factorization: review of existing methods. J. Air Waste Manag. Assoc. 57, 146–154. https://doi.org/10.1080/10473289.2007.10465319.
Reizer, M., Calzolai, G., Maciejewska, K., Orza, J.A.G., Carraresi, L., Lucarelli, F., Juda-rezler, K., 2021. Measurement report : receptor modelling for source identification of urban fine and coarse particulate matter using hourly elemental composition. Atmos. Chem. Phys. Discuss.
Richard, A., Gianini, M.F.D., Mohr, C., Furger, M., Bukowiecki, N., Minguillon, M.C., Lienemann, P., Flechsig, U., Appel, K., DeCarlo, P.F., Heringa, M.F., Chirico, R., Baltensperger, U., Prevot, A.S.H., 2011. Source apportionment of size and time resolved trace elements and organic aerosols from an urban courtyard site in Switzerland. Atmos. Chem. Phys. 11, 8945–8963. https://doi.org/10.5194/acp-11-8945-2011.
Rigler, M., Drinovec, L., Lavri, G., Vlachou, A., Prevot, A.S.H., Luc Jaffrezo, J., Stavroulas, I., Sciare, J., Burger, J., Kranjc, I., Turšič, J., Hansen A, D.A., Mocnik, G., 2020. The new instrument using a TC-BC (total carbon-black carbon) method for the online measurement of carbonaceous aerosols. Atmos. Meas. Tech. 13, 4333–4351. https://doi.org/10.5194/amt-13-4333-2020.
Rodriguez, S., Querol, X., Alastuey, A., Kallos, G., Kakaliagou, O., 2001. Saharan dust contributions to PM10 and TSP levels in Southern and Eastern Spain. Atmos. Environ. 35, 2433–2447. https://doi.org/10.1016/S1352-2310(00)00496-9.

Rohr, A.C., Wyzga, R.E., 2012. Attributing health effects to individual particulate matter constituents. Atmos. Environ. 62, 130–152. https://doi.org/10.1016/j.atmosenv.2012.07.036.

Rolph, G., Stein, A., Stunder, B., 2017. Real-time environmental applications and display system: ready. Environ. Model. Software 95, 210–228. https://doi.org/10.1016/j.envsoft.2017.06.025.

Schauer, J.J., Lough, G.C., Shafer, M.M., Christensen, W.F., Arndt, M.F., DeMinter, J.T., Park, J.S., 2006. Characterization of metals emitted from motor vehicles. Res. Rep. Health Eff. Inst.

Seibert, P., Kromp-Kolb, H., Baltensperger, U., Jost, D.T., Schwikowski, M., 1994. Trajectory analysis of high-alpine air pollution data. In: Gryning, S.-E., Millan, M.M. (Eds.), Air Pollution Modeling and its Application X. Springer, US, Boston, MA, pp. 595–596.

Seinfeld, J.H., Pandis, S.N., 1998. Atmospheric chemistry and physics From Air Pollution to Climate Change (Second). John Wiley & Sons, INC.

Smith, S.J., Bond, T.C., 2014. Two hundred fifty years of aerosols and climate : the end of the age of aerosols. Atmos. Chem. Phys. 14, 537–549. https://doi.org/10.5194/acp-14-537-2014.

Stefenelli, G., Pospisilova, V., Lopez-Hilfiker, F.D., Daellenbach, K.R., Hüglin, C., Tong, Y., Baltensperger, U., Prevot, A.S.H., Slowik, J.G., 2019. Organic aerosol source apportionment in Zurich using an extractive electrospray ionization time-of-flight mass spectrometer (EESI-TOF-MS) - Part 1: biogenic influences and day-night chemistry in summer. Atmos. Chem. Phys. 19, 14825–14848. https://doi.org/10.5194/acp-19-14825-2019.

Stein, A.F., Draxler, R.R., Rolph, G.D., Stunder, B.J.B., Cohen, M.D., Ngan, F., 2015. Noaa's hysplit atmospheric transport and dispersion modeling system. Bull. Am. Meteorol. Soc. 96, 2059–2077. https://doi.org/10.1175/BAMS-D-14-00110.1.

Tanda, S., Ličbinský, R., Hegrová, J., Goessler, W., 2019. Impact of New Year's Eve fireworks on the size resolved element distributions in airborne particles. Environ. Int. 128, 371–378. https://doi.org/10.1016/j.envint.2019.04.071.

Tobler, A., Bhattu, D., Canonaco, F., Lalchandani, V., Shukla, A., Thamban, N.M., Mishra, S., Srivastava, A.K., Bisht, D.S., Tiwari, S., Singh, S., Močnik, G., Baltensperger, U., Tripathi, S.N., Slowik, J.G., Prévôt, A.S.H., 2020. Chemical characterization of PM2.5 and source apportionment of organic aerosol in New Delhi, India. Sci. Total Environ. 745, 1–12. https://doi.org/10.1016/j.scitotenv.2020.140924.

Tremper, A.H., Font, A., Priestman, M., Hamad, S.H., Chung, T.C., Pribadi, A., Brown, R. J.C., Goddard, S.L., Grassineau, N., Petterson, K., Kelly, F.J., Green, D.C., 2018. Field and laboratory evaluation of a high time resolution x-ray fluorescence instrument for determining the elemental composition of ambient aerosols. Atmos. Meas. Tech. 11, 3541–3557. https://doi.org/10.5194/amt-11-3541-2018.

Vasilatou, V., Manousakas, M., Gini, M., Diapouli, E., Scoullos, M., Eleftheriadis, K., 2017. Long term flux of saharan dust to the aegean sea around the attica region, Greece. Front. Mar. Sci. 4, 42. https://doi.org/10.3389/fmars.2017.00042.

Vecchi, R., Bernardoni, V., Cricchio, D., D'Alessandro, A., Fermo, P., Lucarelli, F., Nava, S., Piazzalunga, A., Valli, G., 2008. The impact of fireworks on airborne particles. Atmos. Environ. 42, 1121–1132. https://doi.org/10.1016/j.atmosenv.2007.10.047.

Vejahati, F., Xu, Z., Gupta, R., 2010. Trace elements in coal: associations with coal and minerals and their behavior during coal utilization - a review. Fuel 89, 904–911. https://doi.org/10.1016/j.fuel.2009.06.013.

Viana, M., Kuhlbusch, T.a.J., Querol, X., Alastuey, A., Harrison, R.M., Hopke, P.K., Winiwarter, W., Vallius, M., Szidat, S., Prévôt, A.S.H., Hueglin, C., Bloemen, H., Wåhlin, P., Vecchi, R., Miranda, A.I., Kasper-Giebl, A., Maenhaut, W., Hitzenberger, R., 2008. Source apportionment of particulate matter in Europe: a review of methods and results. J. Aerosol Sci. 39, 827–849. https://doi.org/10.1016/j.jaerosci.2008.05.007.

Viana, M., Reche, C., Amato, F., Alastuey, a., Querol, X., Moreno, T., Lucarelli, F., Nava, S., Calzolai, G., Chiari, M., Rico, M., 2013. Evidence of biomass burning aerosols in the Barcelona urban environment during winter time. Atmos. Environ. 72, 81–88. https://doi.org/10.1016/j.atmosenv.2013.02.031.

Visser, S., Slowik, J.G., Furger, M., Zotter, P., Bukowiecki, N., Canonaco, F., Flechsig, U., Appel, K., Green, D.C., Tremper, A.H., Young, D.E., Williams, P.I., Allan, J.D., Coe, H., Williams, L.R., Mohr, C., Xu, L., Ng, N.L., Nemitz, E., Barlow, J.F., Halios, C. H., Fleming, Z.L., Baltensperger, U., Prévôt, A.S.H., 2015. Advanced source apportionment of size-resolved trace elements at multiple sites in London during winter. Atmos. Chem. Phys. 15, 11291–11309. https://doi.org/10.5194/acp-15-11291-2015.

Wang, H., Miao, Q., Shen, L., Yang, Q., Wu, Y., Wei, H., 2021. Air pollutant variations in Suzhou during the 2019 novel coronavirus (COVID-19) lockdown of 2020: high time-resolution measurements of aerosol chemical compositions and source apportionment. Environ. Pollut. 271, 116298. https://doi.org/10.1016/j.envpol.2020.116298.

Wang, Q., Qiao, L., Zhou, M., Zhu, S., Griffith, S., Li, L., Yu, J.Z., 2018. Source apportionment of PM2.5 using hourly measurements of elemental tracers and major constituents in an urban environment: investigation of time-resolution influence. J. Geophys. Res. Atmos. 123, 5284–5300. https://doi.org/10.1029/2017JD027877.

Yu, Y., He, S., Wu, X., Zhang, C., Yao, Y., Liao, H., Wang, Q., Xie, M., 2019. PM2.5 elements at an urban site in Yangtze River Delta, China: high time-resolved measurement and the application in source apportionment. Environ. Pollut. 253, 1089–1099. https://doi.org/10.1016/j.envpol.2019.07.096.

Zhuang, H., Chan, C.K., Fang, M., Wexler, A.S., 1999. Formation of nitrate and non-sea-salt sulfate on coarse particles. Atmos. Environ. 33, 4223–4233. https://doi.org/10.1016/S1352-2310(99)00186-7.

Zotter, P., Ciobanu, V.G., Zhang, Y.L., El-Haddad, I., Macchia, M., Daellenbach, K.R., Salazar, G.A., Huang, R.J., Wacker, L., Hueglin, C., Piazzalunga, A., Fermo, P., Schwikowski, M., Baltensperger, U., Szidat, S., Prévôt, A.S.H., 2014. Radiocarbon analysis of elemental and organic carbon in Switzerland during winter-smog episodes from 2008 to 2012-Part 1: source apportionment and spatial variability. Atmos. Chem. Phys. 14, 13551–13570. https://doi.org/10.5194/acp-14-13551-2014.

Zotter, P., Herich, H., Gysel, M., El-Haddad, I., Zhang, Y., Mocnik, G., Hüglin, C., Baltensperger, U., Szidat, S., Prévôt, A.S.H., 2017. Evaluation of the absorption Ångström exponents for traffic and wood burning in the Aethalometer-based source apportionment using radiocarbon measurements of ambient aerosol. Atmos. Chem. Phys. 17, 4229–4249. https://doi.org/10.5194/acp-17-4229-2017.